JAMES | Journal of Advances in Modeling Earth Systems

RESEARCH ARTICLE
10.1029/2023MS004171

Systematic Regional Aerosol Perturbations (SyRAP) in Asia Using the Intermediate-Resolution Global Climate Model FORTE2

Camilla W. Stjern[1], Manoj Joshi[2], Laura J. Wilcox[3], Amee Gollop[3], and Bjørn H. Samset[1]

[1]CICERO Center for International Climate Research, Oslo, Norway, [2]University of East Anglia, Norwich, England, [3]National Centre for Atmospheric Science, University of Reading, Reading, England

Key Points:

- Removing emissions of absorbing aerosols over both East Asia and South Asia is projected to cause a local drying
- In certain subregions, the impact of SO_4 on precipitation is strongly dependent on the background climate state
- Results show regionally linear responses in temperature and precipitation and can be used as input to emulators and simple climate models

Supporting Information:

Supporting Information may be found in the online version of this article.

Correspondence to:

C. W. Stjern,
camilla.stjern@cicero.oslo.no

Citation:

Stjern, C. W., Joshi, M., Wilcox, L. J., Gollop, A., & Samset, B. H. (2024). Systematic Regional Aerosol Perturbations (SyRAP) in Asia using the intermediate-resolution global climate model FORTE2. *Journal of Advances in Modeling Earth Systems*, *16*, e2023MS004171. https://doi.org/10.1029/2023MS004171

Received 22 DEC 2023
Accepted 31 AUG 2024

Author Contributions:

Conceptualization: Manoj Joshi, Laura J. Wilcox, Bjørn H. Samset
Data curation: Manoj Joshi
Funding acquisition: Bjørn H. Samset
Investigation: Manoj Joshi, Laura J. Wilcox, Amee Gollop, Bjørn H. Samset
Methodology: Manoj Joshi, Laura J. Wilcox
Project administration: Bjørn H. Samset
Resources: Manoj Joshi
Software: Manoj Joshi

Abstract Emissions of anthropogenic aerosols are rapidly changing, in amounts, composition and geographical distribution. In East and South Asia in particular, strong aerosol trends combined with high population densities imply high potential vulnerability to climate change. Improved knowledge of how near-term climate and weather influences these changes is urgently needed, to allow for better-informed adaptation strategies. To understand and decompose the local and remote climate impacts of regional aerosol emission changes, we perform a set of Systematic Regional Aerosol Perturbations (SyRAP) using the reduced-complexity climate model FORTE 2.0 (FORTE2). Absorbing and scattering aerosols are perturbed separately, over East Asia and South Asia, to assess their distinct influences on climate. In this paper, we first present an updated version of FORTE2, which includes treatment of aerosol-cloud interactions. We then document and validate the local responses over a range of parameters, showing for instance that removing emissions of absorbing aerosols over both East Asia and South Asia is projected to cause a local drying, alongside a range of more widespread effects. We find that SyRAP-FORTE2 is able to reproduce the responses to Asian aerosol changes documented in the literature, and that it can help us decompose regional climate impacts of aerosols from the two regions. Finally, we show how SyRAP-FORTE2 has regionally linear responses in temperature and precipitation and can be used as input to emulators and tunable simple climate models, and as a ready-made tool for projecting the local and remote effects of near-term changes in Asian aerosol emissions.

Plain Language Summary Emissions of anthropogenic aerosols are rapidly changing, both in amounts, composition, and geographical distribution. Aerosol-climate impacts follow patterns and time evolutions different to those from greenhouse gas-driven surface warming, potentially enhancing climate risk. However, our understanding of these patterns and processes is still limited. In East and South Asia, strong aerosol trends and high population densities imply a high potential vulnerability to climate change. To allow for better-informed adaptation strategies, there is an urgent need for improved knowledge of how near-term climate and weather influences these changes. Here we perform a set of Systematic Regional Aerosol Perturbations (SyRAP) using the reduced-complexity climate model FORTE 2 to decompose the climate impacts of regional aerosol emission changes. We developed a new functionality in the model, allowing for the ability to emulate the indirect aerosol effect—in isolation or in combination with aerosol radiation interactions. We investigate the separate roles of both light-absorbing and -scattering aerosols, and the distinct impacts of emission perturbations in East versus South Asia. We find that SyRAP-FORTE2 is able to reproduce the responses to Asian aerosol changes documented in the literature, and that it can help us decompose regional climate impacts of aerosols from the two regions.

1. Introduction

Aerosol emissions have a wide range of impacts on the climate both near to and far from emission sources, spanning from local changes in surface solar radiation and warming to large-scale modifications of atmospheric circulation patterns and monsoon precipitation (Gao et al., 2023; J. Li et al., 2022; Persad et al., 2023). Anthropogenic aerosols have been found to have an outsized near-term influence on extreme events in recent climate model studies (Samset, Sand, et al., 2018). In some regions, anthropogenic aerosol impacts have even been shown to dominate over climate impacts from increasing greenhouse gas emissions (Fahrenbach et al., 2024; Gillett et al., 2004; Monerie et al., 2022; Risser et al., 2024; Westervelt et al., 2020). One such region is South and East Asia, which is highly vulnerable to climate risk due to a high population density, rapid industrial

Supervision: Manoj Joshi, Laura J. Wilcox
Validation: Laura J. Wilcox
Writing – original draft: Manoj Joshi, Laura J. Wilcox, Amee Gollop, Bjørn H. Samset
Writing – review & editing: Manoj Joshi, Laura J. Wilcox, Amee Gollop, Bjørn H. Samset

development, and severe water stress (Giorgi & Gao, 2018; Wang et al., 2021). The region currently suffers the globe's highest loading of anthropogenic aerosols (Zhang et al., 2012), which have impacted several aspects of Asian climate. Increasing aerosol emissions have been a key driver of the weakening East and South Asian Summer monsoon, causing widespread summertime drying (Bollasina et al., 2011; Dong et al., 2019; J. Liu et al., 2017), but have also been linked to increases in extreme precipitation over northwest China (Y. Guo et al., 2022). A significant increase in extreme heat events over China, largely driven by increases in greenhouse gas concentrations, has been moderated by high local anthropogenic aerosol emissions (W. Chen et al., 2019). Local aerosol changes have also been linked to catastrophic floods over the Yangtze basin in southwest China as a result of local atmospheric heating from carbonaceous aerosol (Fan et al., 2015; Menon et al., 2002) and due to recent aerosol reductions reducing surface cooling and leading to increased mesoscale convection (Yang et al., 2022).

Some Asian regions are projected to have potentially large but highly uncertain trends of aerosol emissions in the future (Samset et al., 2019). The strong links between aerosol emissions and Asian climate indicate that future aerosol emission changes are likely to contribute markedly to climate related risk in many highly populated regions (Westervelt et al., 2015; Wilcox et al., 2020). This poses a great adaptation challenge and underlines the urgent need for improved knowledge about the near-term impacts of changes in aerosol emissions.

While observational studies are crucial, a deeper understanding of the processes and mechanisms under different aerosol emission pathways necessitates the use of numerical climate models. Many modeling studies have looked at regional perturbations of different species of anthropogenic aerosols with the aim of characterizing the physical response. However, while there are important, consistent findings across these model studies, the use of different experiment designs can make it difficult to understand the causes of differences in the results. For instance, regional perturbations of black carbon (BC) over Asia in the Precipitation Driver Response Model Intercomparison Project (PDRMIP, Myhre et al. (2017)), involving a tenfold increase in year 2000 BC concentrations in nine earth system models (ESMs), were found to enhance the low-level monsoon circulation and precipitation (Xie et al., 2020). Dong et al. (2016) use the atmospheric component of HadGEM2-ES and remove all SO_2 emissions over Asia, finding the presence of SO_2 to cause local cooling and a weakening of the East Asian monsoon. C. Liu et al. (2023) also consider the fast response to Asian aerosol changes, using the atmospheric component of CESM2. They find East Asian aerosol reductions result in a warmer, wetter eastern China, while East Asian aerosol reductions alongside South Asian increases lead to a warmer but drier eastern China. Westervelt et al. (2018) performed simulations where they remove BC or SO_2 in different regions, including China and India, and looked at responses compared to a year 2000 baseline simulation. Their three ESMs all showed a local increase in precipitation from removing SO_2 over China, while the local response to removing BC over India varied between the models. Using IGCM4—the atmospheric component of FORTE2—Herbert et al. (2022) simulate removal of BC or scattering aerosols in China or India compared to present-day concentrations in an otherwise similar setup. Consistent with Westervelt et al. (2018) they find that removing scattering aerosols over China increases precipitation in the region of aerosol removal, and that removing BC over India causes an insignificant precipitation response.

While the examples above show some robust findings across studies, it is difficult to assess whether differences originate from experiment design or from inherent differences in how the models respond to the forcing. In addition to the challenge of different experiment designs, model complexity also varies between studies. In complex models, where more processes and connections are at play, identifying the physical mechanisms behind a given aerosol signal is more challenging than in simpler models where there are fewer processes involved. For that reason, reduced complexity models—such as FORTE2—are a useful tool for understanding the physical responses we see in ESMs. They also have the added benefit of speed of integration, which allows for more and longer simulations at lower cost. It is critical, however, that all the main mechanisms of aerosol-climate interactions are represented. This notably includes the aerosol-cloud interactions (ACI), which was recently assessed to make up 2/3 of the total anthropogenic aerosol radiative forcing over the historical era (Forster et al., 2021), but which is generally not represented in reduced-complexity climate models (e.g., Nicholls et al., 2020, 2021). Including ACI is also important for capturing the pattern as well as the magnitude of the forcing (Zelinka et al., 2023). In the present study, we therefore update our reduced-complexity model, FORTE2, to include a basic representation of ACI.

Using FORTE2, we perform Systematic Regional Aerosol Perturbations (SyRAP) of two different aerosol types (absorbing and scattering) in two different regions (South and East Asia). The linearity of the simulated climate to the strength of the perturbations can readily be tested and, in situations where it holds, the SyRAP simulations can be summed and combined to provide information on climate responses to combinations of aerosol emissions from different regions.

The climate impact of regional aerosol perturbations (e.g., Persad & Caldeira, 2018), perturbations of different aerosol species (e.g., Myhre et al., 2017), and comparisons of purely radiative responses versus ACI (e.g., Dong et al., 2019) have all been considered in isolation in earlier work. In the framework of the SyRAP concept, we can analyze the relative importance of each of these elements, as well as how they interact, hopefully providing new insight in the topic of regional aerosol impacts.

In the next section we describe the FORTE2 model, the aerosol input data, and how ACI are emulated in the model. Section 3 describes the details of the SyRAP simulation setups. The climatology of FORTE2 is described in Section 4, including an account of its representation of important Pacific circulation patterns. Finally, in Section 5, we present responses in a selection of variables starting with core responses in temperature, precipitation, clouds and dynamics, an account of FORTE2 ACI impacts, regional linearity of the perturbations and dependence on the climate state. Simulations and the general FORTE2 responses are summarized in Section 6.

2. An Updated Version of the FORTE2 Model, and Its Aerosol Representation

2.1. The FORTE2 Model

FORTE 2.0 (FORTE2) is an intermediate-complexity coupled atmosphere–ocean general circulation model (Blaker et al., 2021) consisting of the Intermediate General Circulation Model 4 (Joshi et al., 2015) and the Modular Ocean Model-Array (Webb, 1996). The atmospheric model has a standard T42 resolution and 35 sigma layers, extending up to 0.1 hPa, while the ocean model has 15 vertical layers going down to 5,000 m depth. The atmospheric model has been used in the past in studies of aerosols over Asia (Herbert et al., 2022), and its predecessors have been used to explore climate sensitivity (Forster et al., 2000), the importance of the semi-direct effect of absorbing aerosols (Cook & Highwood, 2004), climate impacts of explosive volcanic eruptions (Highwood & Stevenson, 2003), and precipitation responses to geoengineering (Ferraro et al., 2014).

2.2. The Copernicus Atmosphere Monitoring Service (CAMS) Reanalysis as Aerosol Perturbation Input Data

The global gridded speciated aerosol optical depth (AOD) and vertical distributions used in SyRAP are based on the CAMS reanalysis (CAMSRA; Inness et al., 2019). CAMSRA has an 80 km (T255) horizontal resolution and provided data from 2003 to 2021 at the time of writing. CAMSRA uses cycle 42R1 of the IFS, which includes an interactive aerosol scheme (Morcrette et al., 2009). Anthropogenic emissions of BC, organic carbon, and sulfur dioxide are taken from the MACCity inventory (Granier et al., 2011) for 2003 to 2010. After 2010, emissions were taken from Representative Concentration Pathway 8.5 (Riahi et al., 2011). Biomass burning emissions are from the Global Fire Assimilation System, version 1.2 (GFASv1.2; Kaiser et al., 2012). Dust and sea salt emissions are calculated interactively. The reanalysis assimilates AOD at 550 nm from the Advanced Along-Track Scanning Radiometer (AATSR; Popp et al., 2016), and the Moderate Resolution Imaging Spectroradiometer (MODIS) aboard Terra and Aqua (Levy et al., 2013). CAMSRA has smaller biases relative to independent observations than the Monitoring Atmospheric Composition and Climate reanalysis and CAMS interim analysis (Xian et al., 2023). However, the RCP8.5 emission pathway used from 2010 onwards does not capture the recent rapid reduction in Chinese emissions, instead retaining strong Chinese aerosol emissions and related high aerosol concentrations in the Asian outflow regions. As we are designing idealized simulations with and without regional aerosol perturbations, rather than trying to reproduce the real-world time evolution of Asian aerosol emissions, RCP8.5 is well-suited for our study. For more details of CAMSRA, including key updates compared to previous reanalyses, and an evaluation of the CAMSRA aerosol product compared to previous reanalyses and the Aerosol Robotic NETwork (AERONET; Holben et al., 1998), see Inness et al. (2019).

To produce the SyRAP aerosol perturbations used in the experiments described in Section 3, CAMSRA monthly fields of speciated AOD and 3D mass mixing ratios for 2003–2021 are interpolated to T42 resolution, to produce monthly climatologies of total anthropogenic (BC, OC and SO_4), absorbing (BC and OC), and scattering aerosol

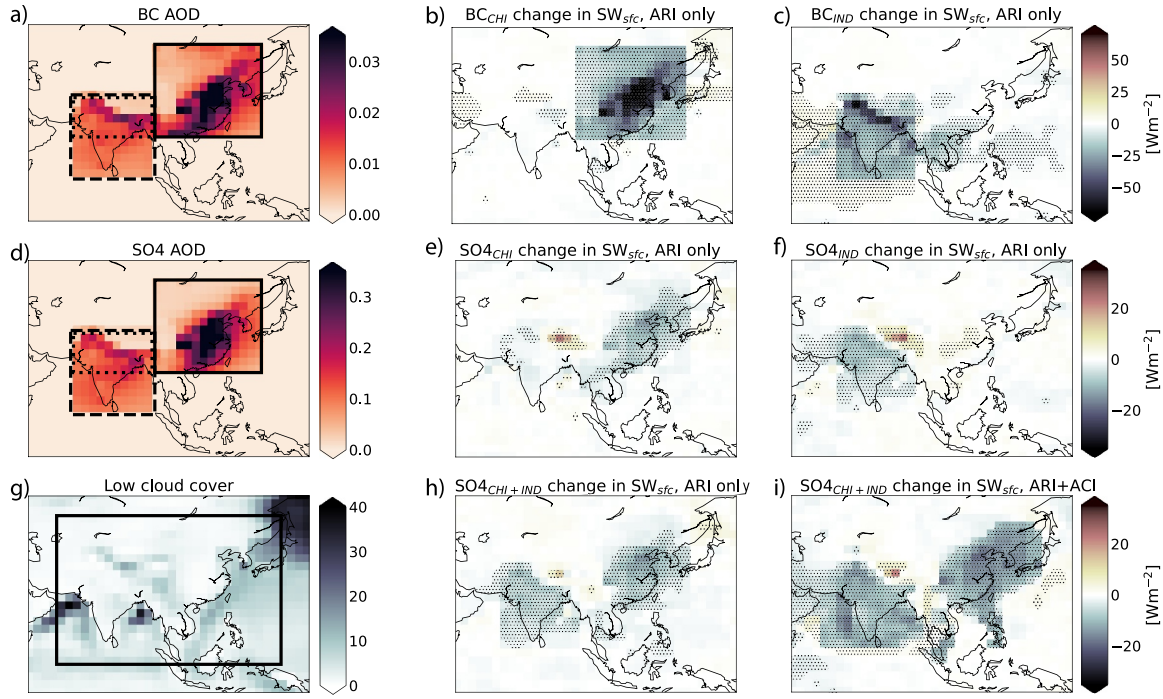

Figure 1. Maps showing the summertime (JJA) anthropogenic aerosol optical depth of (a) black carbon (BC) and OC and (d) SO_4 within the China (CHI, solid) and the India (IND, dashed; NIND, dotted) regions, as well as the JJA ARI-only response in downwelling surface solar radiation (SW_{sfc}) to adding the BC/OC to (b) CHI and (c) IND, and the SO_4 to (e) CHI and (f) IND, respectively. Gray hatching indicates where responses are statistically significant. Panel (g) shows the low cloud cover, with the black frame marking the area for which the aerosol-cloud interactions (ACI) effect is included, and panel (h) shows ARI-impacts of SO_4 on SW_{sfc} in the experiment where we add SO_4 to both CHI and IND. Finally, in panel (i) we show the response in SW_{sfc} but where ACI impacts are also included.

(SO_4) optical depth at each gridpoint. Aerosols are not transported in FORTE2. The aerosols are vertically uniform from the second lowest model layer (σ, or $p/p_{surface} = 0.88$ or approximately 950 m above the surface) until a pressure level p_{min}. p_{min} is defined, for each gridbox, from CAMSRA as 850 hPa or the first pressure level where the 2003–2021 mean mixing ratio of BC + OC + SO_4 falls below 5×10^9 kg kg^{-1}, whichever is smaller. Over topography, an additional p_{min} threshold is set such that $\sigma_{min} < 0.75$ and $p_{min} > 300$ hPa. Typical values of p_{min} are 600 hPa over much of South Asia and 700 hPa over much of East Asia in May. These profiles are then fed into the FORTE2 radiation scheme.

2.3. New Aerosol-Cloud-Interactions in FORTE2

Aerosol-cloud interactions such as aerosol impacts on cloud albedo or lifetime, are not included in the original setup of FORTE2. This means that in most of the FORTE2 experiments performed in this analysis, only the climate responses from aerosol-radiation interactions (ARI)—including the semi-direct effect of BC—are included. However, we include new functionality for SyRAP, used in some of the SO_4 perturbation simulations (Section 3). Within a specified region (Figure 1g), ACI is parameterized when AOD $\tau > 0.07$. The chosen value of τ is based on the AOD and cloud top effective radius changes in Dong et al. (2019). This means that the emulated ACI in FORTE2 follows a similar pattern to the ACI simulated by HadGEM3 in response to an Asian aerosol perturbation. The value of τ determines the spatial pattern of the emulated ACI, rather than its strength, and so represents a balance between capturing the ACI pattern simulated by a CMIP-class model and avoiding activating ACI at every gridpoint within the specified domain.

The strength of the ACI is determined by the effective radius change prescribed in the new functionality. If any of low-level cloud, mid-level cloud, or shallow convective cloud are present, the effective cloud particle radius in those clouds is changed from 15 to 10 mm, the effective radius in FORTE2 is changed from 15 to 10 m, spanning the range of most CMIP5 models for this variable (Wilcox et al., 2015). A test of the sensitivity to this choice is included in the manuscript, where results from an experiment with the effective radius changed from 15 to 13 m is discussed.

Table 1
SyRAP-FORTE Simulations Performed for the Present Study

	BC (ARI only)	SO_4 (ARI only)	SO_4 (ACI only)	SO_4 (ACI and ARI)	Climate states
BASE Global baseline simulation with no aerosols	–	–	–	–	piC, +1 K
IND (India) 65:95°E, 5:35°N	**BC_{IND}** [0.010]	**$SO4_{IND}$** [0.104]	–	–	piC, +1 K
CHI (East China) 95:133°E, 20:53°N	**BC_{CHI}** [0.015]	**$SO4_{CHI}$** [0.126]	–	–	piC, +1 K
IND + CHI	**$BC_{IND+CHI}$** [0.025]	**$SO4_{IND+CHI}$** [0.230]	aci-reff10$_{IND+CHI}$	SO4aci-reff10$_{IND+CHI}$ Changing effective droplet radius from 15 to 10 μm	piC, +1 K
LINEARITY TESTS, smaller India region					
NIND (India) 65:95°E, 20:35°N	BC_{NIND} [0.011]	$SO4_{NIND}$ [0.100]	–	–	piC
NIND + CHI	$BC_{NIND+CHI}$ [0.026]	$SO4_{NIND+CHI}$ [0.226]	–	–	piC
ACI SENSITIVITY TEST, done for IND + CHI					
Changing effective droplet radius from 15 to 13 μm	–	–	aci-reff13$_{IND+CHI}$	SO4aci-reff13$_{IND+CHI}$	piC, +1 K

Note. Each indicated simulation was run for 200 years. Core simulations are shown in bold, the rest are linearity or sensitivity tests. "Climate state" refers to the global mean surface temperature change relative to preindustrial conditions. Numbers in brackets indicate the regional mean AOD of added BC/OC or SO_4. The geographical regions where aerosol optical depth is perturbed are shown in Figure 1a.

A potential caveat in the SyRAP set-up, particularly related to the ACI effect, is the experiment design of a zero-aerosol background. As the susceptibility of clouds to microphysical impacts of aerosols tend to be stronger the cleaner the background (Platnick & Twomey, 1994), this is likely to have some impact on the magnitude of the ACI effects in this study. Note, however, that while this would make the clouds in more complex ESMs including a microphysics scheme extremely susceptible to aerosol perturbations, this is not an issue in the simpler FORTE2, where the magnitude of the ACI effect is designed to be comparable to findings in the literature. Note also that ACI effects are only included in two experiments, as described in the next section. The core experiments in this paper include only aerosol-radiation interactions, which should not be sensitive to the background aerosol level.

3. SyRAP in FORTE2

3.1. Core SyRAP Simulation Overview

In the SyRAP simulations performed here, baseline simulations with no aerosols are compared to perturbation simulations with added absorbing (black carbon, BC, and organic carbon, OC) or scattering (sulfate, SO_4) aerosols over India and surrounding regions ("IND," coordinates 65°E–95°E, 5°–35°N) or over parts of East China and surrounding regions ("CHI," coordinates 95°–133°E, 20°–53°N). IND and CHI are shown as black dashed and solid boxes, respectively, in Figure 1. Aerosols are perturbed separately in either CHI or IND, or over both regions at once (IND + CHI)—see Table 1 for an overview of the perturbations. The experiments adding BC and OC are labeled "BC" for simplicity, and the topmost row indicates whether the given experiment includes ARI-effects only, ACI only, or both ARI and ACI.

The added absorbing (BC and OC) and scattering (SO_4) AODs are shown in Figures 1a and 1d. The regional mean BC + OC AOD added in the BC_{CHI} and BC_{IND} experiments are 0.015 and 0.010, while the regional mean SO_4 AOD added in the $SO4_{CHI}$ and $SO4_{IND}$ experiments are 0.126 and 0.104. To illustrate the first step in the climate response chain—namely how the aerosols influence the direct radiative fluxes—we show in Figure 1 the change in surface short wave radiation from adding BC to CHI (Figure 1b) and to IND (Figure 1c). Figures 1e and 1f show corresponding plots for SO_4 but note that these perturbations do not include ACI effects of SO_4. This, and the fact that BC is strongly absorbing, causes the ARI-only radiation impacts of BC to be considerably stronger than for SO_4. To illustrate this, Figure 1h shows the default (ARI-only) experiment of adding SO_4 to both CHI and IND, while Figure 1i shows the experiment where the ACI effect is included as well, demonstrating a

considerably increased impact on surface SW radiation. Further examples of the impact of the new FORTE2 ACI parameterization will be given in Section 5.2.

3.2. ACI Implementation

In the SyRAP simulations FORTE2 is for the first time set up with the ability to emulate the indirect aerosol effect —in isolation or in combination with ARI. While typically not included in reduced-complexity climate models, ACI account for most of the aerosol forcing globally (Forster et al., 2021; Zelinka et al., 2014), and there are indications that the ACI is important for the Asian response to aerosol specifically (Dong et al., 2019). The scientific body of evidence points toward dynamical rather than thermodynamical mechanisms dominating the aerosol response over Asia (Tian et al., 2018), making it particularly important to get the total aerosol forcing and its geographical pattern right.

The SyRAP ACI simulations allow us to test how important the ACI is for the simulated response to aerosol forcing in this region. The magnitude and pattern of the ACI effect can be easily changed in the model set-up, by scaling the applied effective radius anomaly and scaling the AOD at which cloud changes occur, respectively. This flexibility can be used to provide insight into, for instance, why ESMs differ in their responses to standardized aerosol emission changes. The ACI can be turned on even when the direct aerosol radiative forcing is turned off, so that the effects of nonlinearities when including ACI can be assessed.

Since the ACI effects of aerosol from China and India are hard to disentangle in reality, and as aerosol is not transported in SyRAP, the ACI runs were only done for the experiments perturbing SO_4 in the combined IND + CHI region. For these experiments, ACI is parametrized within a box bounded by coordinates 60°−140°E, 0°–53°N (see box in Figure 1g). The region where ACI is prescribed is chosen to capture regions where significant ACI-induced changes in cloud properties were seen in response to regional aerosol perturbations in HadGEM3 (Dong et al., 2019). In that model, the ACI was shown to be important for the local precipitation response, partly by changing the response in the season when the forcing occurs, and partly by preconditioning the SST pattern that governs the response in later seasons.

As shown in Table 1, we simulate the ACI effect on top of the default radiation-only experiment (SO4aci-reff10$_{IND+CHI}$), but also the ACI-only effect (aci-reff10$_{IND+CHI}$). In addition, we do sensitivity tests reducing the magnitude of the ACI by reducing the effective droplet radius (r_{eff}) from 15 to 13 μm, as opposed to from 15 to 10 μm in the regular ACI runs. These runs will be discussed in Section 5.2.

3.3. Background Climate States

The conditions under which aerosols influence climate are not constant in time. For instance, GHG-induced warming may change cloud distributions and properties, influencing the pattern and magnitude of aerosol forcing, or change the monsoon climatology to which aerosol forcing is being applied, potentially introducing nonlinearities. To understand how aerosol impacts depend on global warming level, we perform all aerosol perturbations in different baseline climates: one with preindustrial CO_2 levels (280 ppmv, piC) and one with approximately present-day CO_2 levels for which climate is about 1° warmer (500 ppmv, +1 K). We also did a baseline simulation with future CO_2 levels for which climate is about 2° warmer than preindustrial conditions (850 ppmv, +2 K). The relatively large CO_2 concentrations in the latter two runs reflect the low climate sensitivity of IGCM4 of 2.1 K on doubling CO_2 (Joshi et al., 2015) and subsequent low transient climate response of FORTE2.

In addition to the core experiments, we also perform an additional set of experiments where the IND region is reduced to a much smaller region comprising only the northern parts of India ("NIND," Table 1). This was motivated by the fact that, as will be shown later, we found interesting differences in the regional additivity of aerosol-impacts over China and India compared to a similar study by Herbert et al. (2022). One difference between these studies was that their "India" region was geographically smaller, and so these experiments address the role of the spatial extent of the AOD perturbation to the differences in our results. The NIND region is marked in dotted lines in Figure 1a. These simulations will be discussed further in Section 5.3.

All simulations are run for 200 years, enabling studies of radiative responses over a timescale of <1 year, fast surface ocean responses on timescales of 10–30 years, and slower deeper ocean changes and equilibrium climate responses. All figures in the present analysis show averages for years 51–200, with the first 50 years discarded to

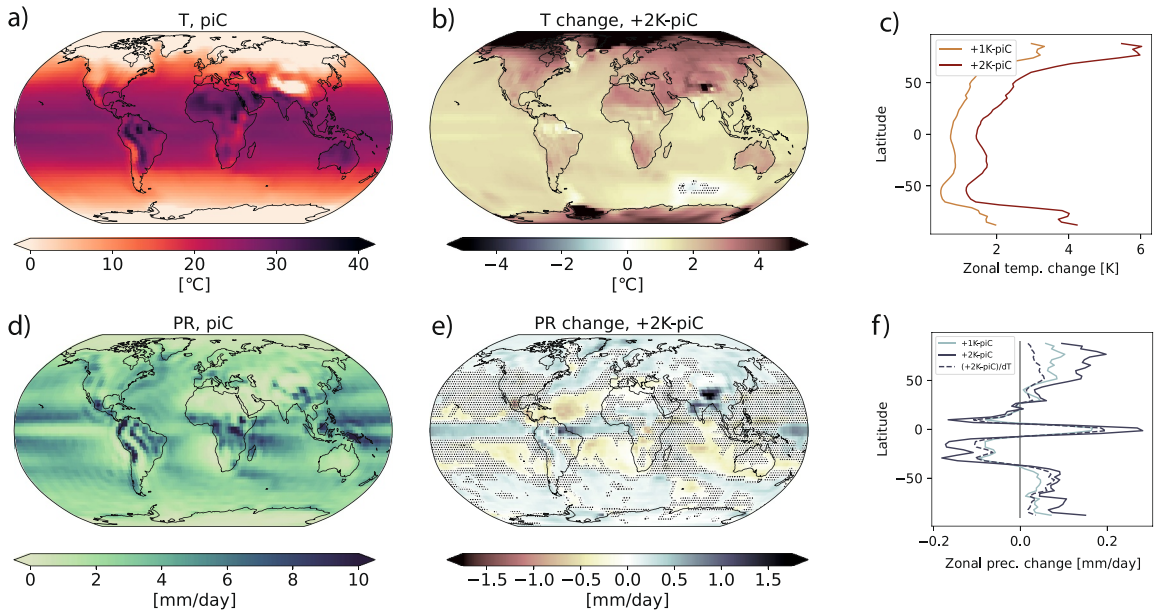

Figure 2. Baseline climatologies (for piC) of annual mean (a) temperature (*T*) and (d) precipitation (PR), as well as geographical patterns of (b) *T* and (e) PR changes for +2 K-piC. Rightmost panels show zonal annual mean changes of (c) *T* and (f) PR. Included in the zonal precipitation panel is also the +2 K-piC precipitation change divided by the global mean +2 K-piC temperature change (dT), illustrating the hydrological sensitivity compared to +1 K-piC. In panels (b) and (e), hatching illustrates non-significant difference.

let the climate state equilibrate. Climate responses are calculated as the mean response for a perturbation experiment minus the mean response for the corresponding baseline simulation. For each grid cell, we perform a two-tailed Student's *t*-test to identify where differences between the baseline and perturbed simulation are statistically significant at the 5% level. In most map plots, we add hatching to areas where changes are *not* statistically significant.

4. FORTE2 Climatological Characteristics

4.1. Baseline Climatology

The climatological distribution of temperature and precipitation in the baseline (piC) simulations are shown in Figures 2a and 2d, respectively. A thorough evaluation of the preindustrial climatology of FORTE2 was conducted in Blaker et al. (2021). Blaker et al. (2021) show that the model's near-surface air temperature compares well to the NOAA-CIRES-DOE Twentieth Century Reanalysis (20CR), both in terms of averages and seasonal variability. The largest biases are cold temperature anomalies over the polar regions and the Himalayas, and a warm anomaly over the Southern Ocean. FORTE2 simulates too little rainfall compared to the 20CR, in particular over the tropical west Pacific, and the South Pacific ITCZ in FORTE2 is too narrow and zonal compared to the reanalysis. While the model performs well in terms of wintertime precipitation over South and East Asia, there is a dry bias in the summer monsoon. Such a bias is typical for the majority of both the CMIP5 and the CMIP6 ensemble (Sperber et al., 2013; Wilcox et al., 2020). The Asian summer monsoon circulation is also too zonal over South East and East Asia, again consistent with the biases seen in CMIP models.

The middle panels of Figure 2 show the climatological differences between +2 K and piC and illustrate how temperature (Figure 2b) and precipitation (Figure 2e) in FORTE2 respond to a strong increase in CO_2. The 2 K global mean surface warming in FORTE2 reproduces known patterns such as an Arctic amplification (Figure 2b), seen also in the zonal mean temperature changes in Figure 2c (in the zonal panels we include differences for both +1 K-piC and +2 K-piC). However, this warming, while causing clear responses in regional precipitation (Figure 2e), produces a global mean precipitation change of only 0.02 mm/day or 0.64%. This gives a hydrological sensitivity (HS) of merely 0.32%/K. In comparison, energy budget constraints dictate a theoretical HS of about 2%/K (M. R. Allen & Ingram, 2002), and the CMIP6 model average HS after 150 years of the 1pctCO2 simulation is 1.6%/K (Norris et al., 2022). There are two main reasons for the low FORTE2 HS. One is the low

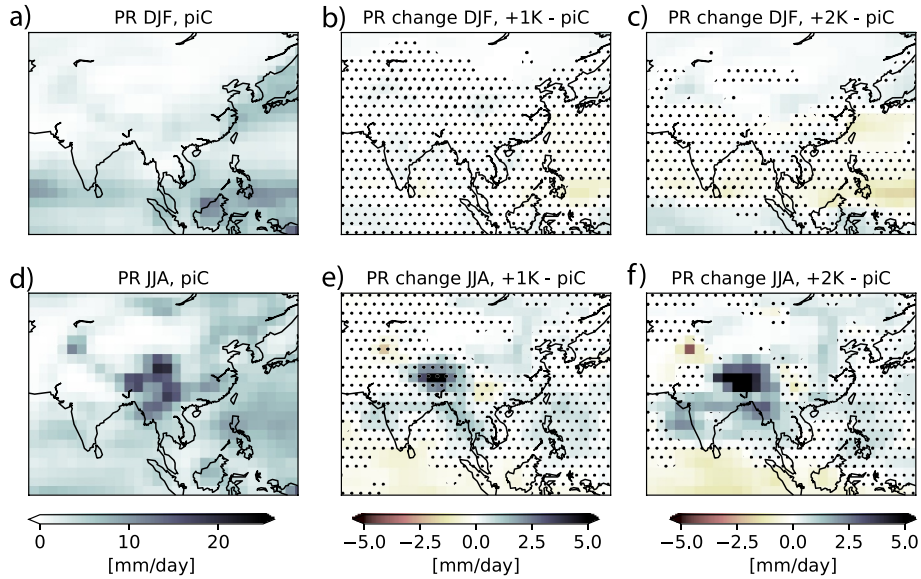

Figure 3. DJF precipitation over Asia for (a) piC, (b) the difference between piC and +1 K, and (c) the difference between piC and +2 K. Corresponding JJA plots are given in panels (d–f), respectively. Maps show averages over simulated years 51–200, and hatching indicates gridcells where the anomalies relative to piC are not significant at the 5% level.

climate sensitivity, which means that the relative increase in CO_2 per Kelvin of warming is high in this model. This, in turn, means that the long wave absorption from CO_2 acts to mute the precipitation increase (Myhre et al., 2018). The other reason is that FORTE2 has a relatively higher fraction of its rain over land, where the HS is markedly lower than the global mean (Samset, Myhre, et al., 2018). While the HS is low, muting the absolute precipitation response to climate forcings, the overall patterns are still in line with expectations when compared for example, to CMIP6 (Tebaldi et al., 2021) or PDRMIP (Samset et al., 2016) responses.

The dashed line in Figure 2f shows the +2 K-piC precipitation change divided by the +2 K-piC global mean temperature difference. As the global mean temperature change between piC and +1 K is by definition around 1 K, we can compare the dashed and the light blue line to see that the precipitation response in the two climate states (+1 K and +2 K) is reasonably linear. This linearity holds when we narrow the zonal averages to the latitudes encompassing only the Asia region (not shown). There are some differences around Southern Hemisphere midlatitudes and at higher Northern Hemisphere latitudes, but the zonal mean precipitation response to warming is very consistent around the latitudes of the region of focus in this study. In Section 5.4 we take a closer look at how aerosol responses may differ when aerosols are added at different global warming levels.

The Asian precipitation response to +1 K and +2 K warming is shown in Figure 3. In winter, there is little precipitation during the winter monsoon, and the precipitation response to warming is also small. In summer, global warming results in increased precipitation over most of Asia. Note, however, that while Figure 2f suggested a linear precipitation increase from +1 K to +2 K, the geographical patterns in Figure 3 do not show such linearity over for instance Northeast China. The pattern of the precipitation increase in +2 K reflects the climatological precipitation pattern, with the maximum increase located in the region of the maximum precipitation in piC.

Zooming in on the region of interest in this paper, we show in Figure 4 climatological (piC) surface pressure and 850 hPa wind for the summer (JJA) and winter (DJF) months, respectively. FORTE2 is compared to ERA5 reanalysis (Hersbach et al., 2020), averaged over the 1940–2022 period. The direction of the monsoon flow over South Asia is well captured by FORTE2. However, the flow is too weak over India and the Bay of Bengal, and is too zonal over Southeast Asia. The zonal flow over Southeast Asia, and an easterly bias in the location of the West North Pacific Subtropical High contribute to a dry bias over northeastern China. Most of the Asian summer monsoon precipitation in FORTE2 falls over Myanmar and southern China (Figure 3d), while India and northeastern China are too dry. Such dry biases are common in CMIP6 models (Wilcox et al., 2020). However, the

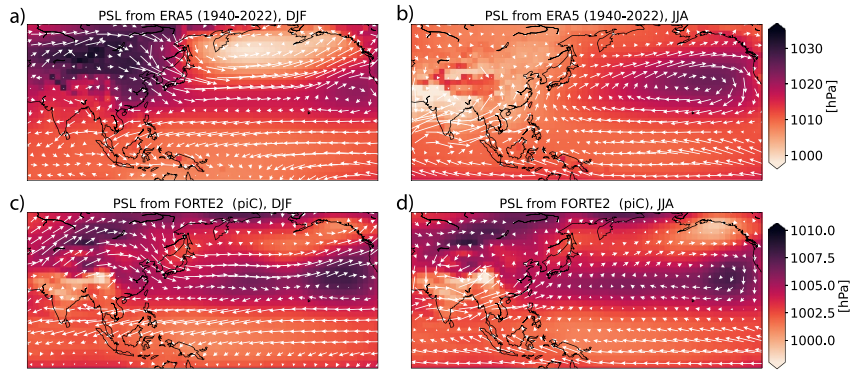

Figure 4. Mean sea level pressure and 850 hPa winds (arrows) for ERA5 (averaged over 1940–2022) for (a) DJF and (b) JJA, and for FORTE2 piC (years 51–200) for (c) DJF and (c) JJA. Note that color scale limits are different between ERA5 and FORTE.

atmosphere component of FORTE, IGCM4, has been shown to reproduce the observed seasonal cycle in precipitation well (Herbert et al., 2022).

In winter, the Aleutian low is too weak in FORTE2 compared to ERA5. Combined with a low pressure bias over land, this causes the East Asian Winter Monsoon to also be too weak, although the direction of the flow over northeast Asia is in good agreement with the reanalysis. The seasonal variation in sea level pressure over Asia is small in FORTE2 compared to ERA5, which is largely due to the pressure over land being too high in winter.

4.2. Pacific Ocean Response

Due to the proximity of the perturbation zones to the Pacific region it is useful to assess the Pacific climatological state across the baseline climates. If differences are found between the baselines (i.e., between piC, +1 K and +2 K) due to different CO_2 loadings, they are likely to modify the Asian responses to regional aerosol perturbations at the different warming levels, as changes in the Pacific circulation are an important part of the response to Asian aerosol forcing (e.g., Dong et al., 2019; Wilcox et al., 2019; Williams et al., 2022).

Standard deviations of the Niño 3.4 index are presented in Table 2 (column three) and remain within a 0.01 tolerance of one another; FORTE2's Nino 3.4 variance is on the weaker end of CMIP6 models, though not an outlier (S. Chen et al., 2023). ENSO frequency is between 2 and 3 years for each baseline, which is consistent with the observed ENSO occurrence of around once every 2–7 years (R. J. Allen, 2000). Table 2 demonstrates that broadly speaking, variability over this key dynamical region is insensitive to changes in the global warming level. Analysis is repeated for the Niño 3 index (column two) and confirms that the Pacific climatological state is insensitive to CO_2 loading.

The large-scale SST patterns and associated winter precipitation anomalies for El Niño and La Niña composites from the piC baseline are presented in Figure 5. This analysis was repeated for the +1 K and +2 K baselines and the large-scale structures remain consistent across all three baseline climates (not shown). The spatial structures of both El Niño and La Niña SST composites are consistent with events captured in the Extended Reconstructed SST version 3b (ETSSTv3b) reanalysis over the period 1949 to 2015 (see B. Li et al., 2018). Notable differences are: in the El Niño composite, Figure 5a, the magnitude of SST anomaly is around 30% weaker on the equatorial South American coastline, and in the La Niña composite the cold anomaly extends too far toward the Maritime

Table 2
ENSO Related Statistics Including the Two Commonly Used Niño Regions and a Breakdown of the Number and Type of ENSO Events in the Three Systematic Regional Aerosol Perturbations FORTE2 Baseline Climates

Experiment	Niño 3 index standard deviation	Niño 3.4 index standard deviation	Number of El Niño events	Number of La Niña events
piC	0.52	0.59	15	16
+1 K	0.53	0.58	17	23
+2 K	0.52	0.58	16	21

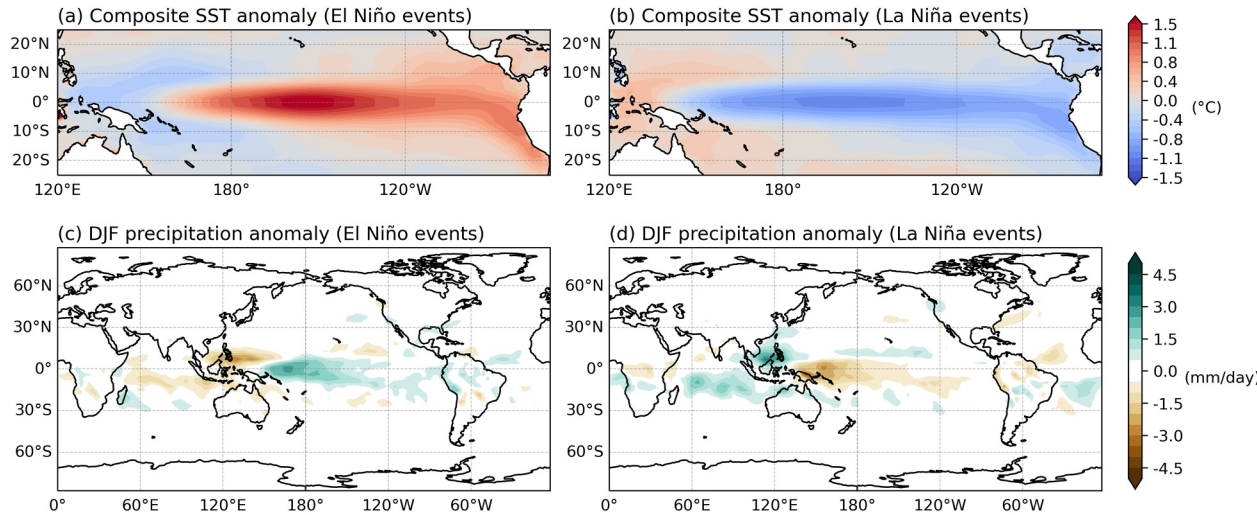

Figure 5. (Top Row) Composite anomalies of monthly sea surface temperature during (a) El Niño and (b) La Niña events. (Bottom Row) Winter, DJF, precipitation anomalies for (c) El Niño and (d) La Niña years. Precipitation anomalies with a magnitude of less than 0.5 mm/day are in white. Data from piC baseline only.

continent. Anomaly peak strength is weaker than observed, around 35% and 45% weaker for the El Niño and La Niña composites respectively, consistent with Blaker et al. (2021).

Winter precipitation patterns during ENSO years are consistent with literature (Davey et al., 2014) over the Pacific and maritime continent. Expected remote precipitation impacts, such as a drying signal over southern Africa in El Niño winters (Figure 5c) and a drying tendency stretching toward India in the La Niña winters (Figure 5d) are captured but are weak. Some remote signals, such as that over Europe, are not captured. FORTE2 is showing some promise in simulating the teleconnections associated with ENSO but this remains an active area for further investigation and model development.

Overall, ENSO events occur with a good frequency but are weaker than observed; particularly La Niña events are short lived and lack strength. ENSO frequency, biases and teleconnections are consistent over all three global warming levels, giving us confidence that any ENSO changes in SyRAP are primarily due to aerosol perturbations, regardless of warming level.

5. Results

5.1. Climate Responses to Individual Aerosol Perturbations

In both IND and CHI, the presence of BC causes strong local reductions of up to 75 Wm^{-2} in downwelling surface solar radiation at the surface (Figures 1b and 1c). Similar albeit much weaker reductions (recall that ACI are not included in these core experiments) are seen for the SO_4 perturbations (Figures 1e and 1f). These radiative perturbations trigger thermodynamic responses which manifest as (rapid) changes in near-surface temperature, surface fluxes, precipitation, and clouds, but they also influence the atmospheric circulation patterns in the region, including the Asian Summer Monsoon.

As all types of aerosols block sunlight from the surface, the dominant local response of adding BC or SO_4 to India or China is a statistically significant cooling (Figure 6)—a JJA cooling from BC/SO_4 of −0.63/−0.16 K over China (Figures 6a and 6b), and −0.54/−0.46 K over India (Figures 6c and 6d). Emissions of SO_4 over China trigger a strong cooling effect over India (Figure 6b). The geographical map of this temperature effect (Figure 7d) shows it to be extremely localized over the northern edge of the India box. This strong cooling is associated with the dynamical response to $SO4_{CHI}$, seen as anomalous descent over the region (see the anomalous divergence in Figure 7o). While this dynamical response dominates the Indian mean response, over most of India there is very little temperature change in response to $SO4_{CHI}$, and local scattering aerosol changes are more important.

A significant remote effect is also seen for BC over China, which causes significant summertime warming over the USA (Figure 6a). Warming of the US in response to Asian aerosol increases has been found earlier in both the

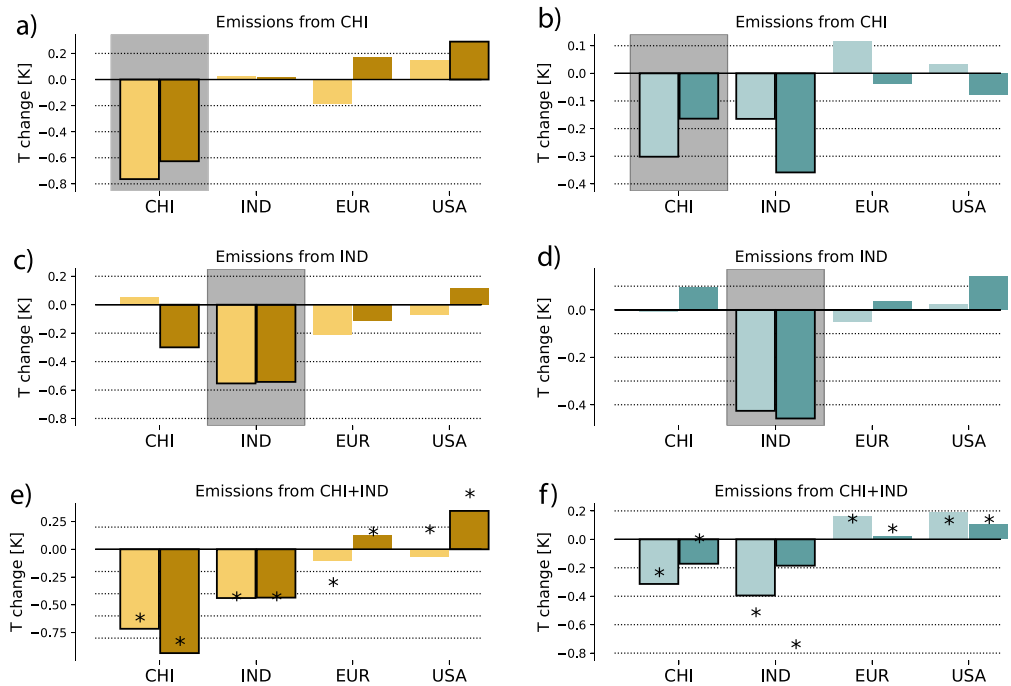

Figure 6. Local (gray background) and remote impacts on regional mean near-surface temperature (K) in the experiments involving adding (a) black carbon (BC) to CHI, (b) SO_4 to CHI, (c) BC to IND, (d) SO_4 to IND, (e) BC to CHI + IND and (f) SO_4 to CHI + IND. Light bars show wintertime (DJF) temperature changes, while dark bars show summertime (JJA) changes. Framed bars indicate where changes are statistically significant, and star symbols in the lowermost row show the summed responses ($BC_{CHI} + BC_{IND}$) or ($SO4_{CHI} + SO4_{IND}$)—responses being linear where bars and stars are comparable in magnitude. We use years 51–200 of the simulation in the analysis.

winter (Wilcox et al., 2019) and annual (Dittus et al., 2021) means in HadGEM3, associated with a weakening of the Aleutian low. FORTE also simulates widespread US warming in response to Chinese BC increases in both seasons, although it is only significant in the regional mean in JJA. This warming is part of a large-scale circulation response due to a Rossby wave train originating in the West Pacific. This response does not project as strongly onto the Aluetian low in FORTE2 as it does in HadGEM3, but some model diversity in the structure of the circulation response is to be expected, and is consistent with the behavior of CMIP-class models (for instance, R. J. Allen and Zhao (2022) find a Rossby wave originating from the tropical Pacific is the driver of the US response to Asian aerosol changes).

Regional mean precipitation responses (Figure S1 in Supporting Information S1) are less clear, partly because the precipitation changes are not uniform in sign across the regional boxes. The regional mean precipitation responses to aerosol involve local drying, but as will be seen below there are significant non-local responses in particular over South Asia. Comparing precipitation responses from the CHI + IND experiment to the all-Asia perturbations of absorbing or scattering aerosols in Herbert et al. (2022), we see that both these studies find a summertime drying over India in response to absorbing aerosols over the larger region. However, while the perturbations cause a significant precipitation increase over China in Herbert et al., we find that Asian absorbing aerosols cause significant drying also over China. Similarly, SO_4 emissions over CHI + IND trigger drying over both regions in FORTE2, while Herbert et al. (2022) find scattering aerosols to cause drying over parts of India but a precipitation increase over China in IGCM4.

Figure 7 shows the geographical pattern of the summer (JJA) responses in near-surface temperature, precipitation, convective clouds and wind speed and direction. The addition of BC over China results in near-surface cooling. This cooling averages to −0.63 K over the CHI region as a whole (Figure 6a), but is largely located to the north of the Yangtze river (Figure 7a), where the largest reductions in downwelling shortwave radiation at the surface are found (Figure 1b). Precipitation south of the Yangtze decreases (Figure 7e), associated with a strong reduction in convective cloud there (Figure 7i). Adding BC over India also results in a cooling co-located with the change in AOD, but the strongest cooling in this case is seen over southeast Asia (Figure 7b), where there is also a large

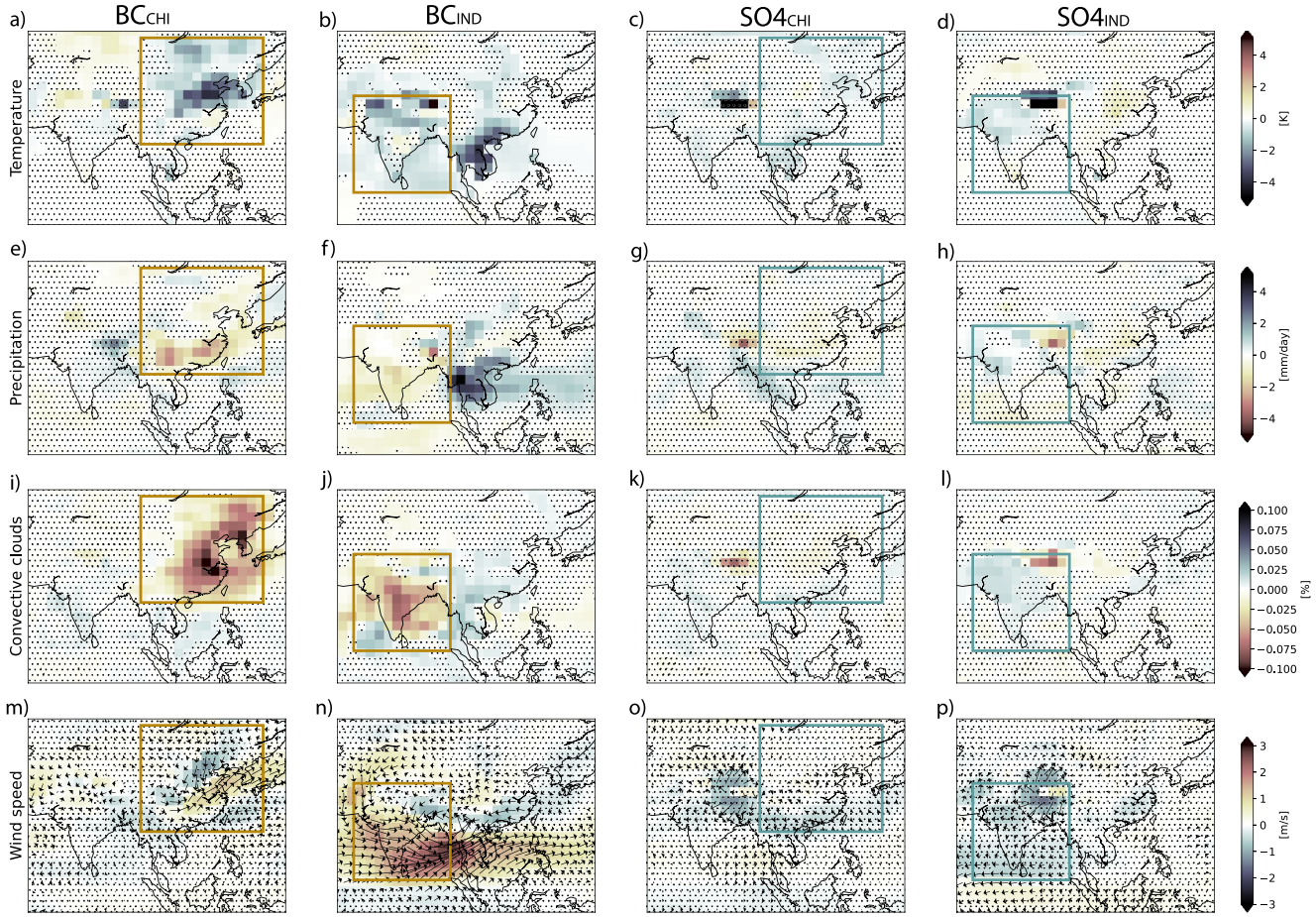

Figure 7. Mean summer (JJA) responses in near-surface temperature, precipitation, convective clouds and 850 hPa wind over the Asian region. Solid brown and blue squares mark the region where black carbon or SO_4 is perturbed, respectively. Maps are based on years 51–200 of the simulations, and hatched regions show areas where differences from the baseline are not statistically significant (by Student's *t*-test, *p*-value 0.05).

increase in precipitation (Figure 7f) due to an increase in the strength of the monsoon flow from the Bay of Bengal (Figure 7n). However, as in the BC_{CHI} case, precipitation and convective clouds (Figure 7j) decrease over the perturbation region due to the combined impact of reduced surface temperatures and increased atmospheric temperatures in response to the absorbing aerosol (see maps of temperature changes at the 850 hPa level in Figure S2 in Supporting Information S1), which has a strong stabilizing effect on the atmosphere.

The presence of SO_4 also cools the surface, though not as strongly as for BC for the SyRAP perturbations. In $SO4_{CHI}$, the cooling is only significant over southeast Asia and northeast Asia (Figure 7c). Drying is seen over eastern China, but it is again weaker than in response to BC increases, consistent with a weaker circulation response (Figure 7o). Significant cooling is seen in the northwest of the perturbation domain for $SO4_{IND}$ (Figure 7d), co-located with the largest reductions in downwelling shortwave at the surface (Figure 1f). This cooling results in a weaker South Asian summer monsoon circulation (Figure 7p), and a reduction in precipitation in the northwest of the region (Figure 7h). Precipitation and convective cloud increase in the northeast of the perturbation region (Figure 7l). Increasing scattering aerosol over South Asia also results in a weakened East Asian summer monsoon, which results in significant warming and drying over eastern China.

Both observations and modeling studies indicate that the drying of the Asian summer monsoon seen over the past decades can be linked to increasing concentrations of anthropogenic aerosols (X. Li et al., 2015; Y. Liu et al., 2019; Tian et al., 2018). The SyRAP-FORTE2 simulations presented here allow us to decompose and understand contributions from different regions or aerosol species to the total response. As shown in Section 4, FORTE2 reproduces the important features of Asian climate. To confirm that it also has aerosol-driven climate responses consistent with more complex climate models, and thus can be used to explain the decomposition of the

response into the main drivers (BC vs. SO_4 or India vs. China), we can compare the responses above to those from ESM simulations. Note that even among ESMs, the response to aerosol forcing varies strongly between individual models (R. J. Allen et al., 2020; Samset et al., 2016), which means that we do expect there to be some differences between FORTE and other studies.

While most literature on the monsoon response to aerosol focuses on global all anthropogenic aerosol perturbations (Salzmann et al., 2014; Song et al., 2014; Wilcox et al., 2020), some regional aerosol ESM studies exist (see Section 1), for instance based on PDRMIP (Xie et al., 2020, 2022). We find that the Asian JJA precipitation response to combined India and China BC ($BC_{IND + CHI}$) is comparable to the multi-model mean MJJAS response of 7 PDRMIP models to a tenfold increase of BC over Asia (Xie et al., 2020). Although set-ups between these two studies are different in many aspects, including different baseline climates (preindustrial vs. present-day) and a much stronger perturbation in the latter case, both FORTE2 and PDRMIP simulations display a BC-induced increase in precipitation over India, although PDRMIP result indicate a drying over Southeast Asia that we do not see. The cooling seen over India in our simulations is found in eight out of nine models in the PDRMIP simulations, but the more widespread cooling over East Asia is only seen in a few of the models. Similarly, the impact of regional PDRMIP perturbations of Asian SO_4 on precipitation is studied by Xie et al. (2022), who find a drying of much of the Asian continent but an increase in summer precipitation over arid Central Asia. In FORTE2, the sulfate response is also a drying over much of the region, but the Central Asian JJA precipitation increase extends down to northern India. Recchia and Lucarini (2023) find BC over China to cause local drying but wettening over India and surrounding parts of China, consistent with our findings, as do Krishnamohan et al. (2021) who perform strong BC perturbations in a global climate model and find that local BC enhancement causes a drying over India while BC in China increases India precipitation.

5.2. ACI Responses

The new ACI setup allows us to simulate the separate impacts of direct ARI only (the default simulation set-up), the indirect (ACI) effect only, or the simultaneous impact of both effects. Figure 8 shows the impacts of direct and indirect aerosol effects on temperature, precipitation, and SW ERF. The direct effect of sulfate causes an average (over the ACI region shown in Figure 1g) SW ERF of -1.61 W/m^2, while the indirect effect yields a response of -2.16 W/m^2, see Table 3. While the direct effect cools most areas over Asia (Figure 8a), the indirect effect causes a strong warming over southern parts of India and the region around Thailand (Figure 8d), which is similar to the CMIP6 forcing pattern shown in Figure 7 of Zelinka et al. (2023). The contrast between direct and indirect effects of Asian sulfate is particularly stark in the precipitation response (Table 3), and Figure 8b versus Figure 8e shows that these differences largely originate in the regions for which the ACI trigger warming.

Compared to the CMIP5 ensemble (Zelinka et al., 2014), FORTE2 has a similar spatial extent of the ACI-driven SW forcing (Figure 8f). In CMIP5, the maximum negative ACI forcing from scattering aerosols is located north of Indonesia, a pattern that is largely reproduced in FORTE2, albeit with a relatively strong forcing also over Indian land regions. Dong et al. (2019), performing simulations with HadGEM3 with and without the ACI effect, find a much more complex ACI forcing pattern, with positive SW forcing over India and negative over China. In terms of the relative importance of ACI versus ARI, both (Zelinka et al., 2014) and Dong et al. (2019) are consistent with the present study in that ACI exert the strongest radiative impact in the region. Dong et al. (2019) found that ARI resulted in weak circulation and precipitation changes, and that ACI was the dominant driver of monsoon changes. An important part of this mechanism, however, was the ACI-induced warming in Maritime Continent SST, which is not something we see in FORTE2. The precipitation response pattern of Dong et al. (2019) is also very different from FORTE2, with an increase in South Asian and decrease in East Asian precipitation. The comparison of L. Guo et al. (2015) showing differences in Asian precipitation patterns between CMIP5 models with and without ACI, however, is more consistent with FORTE2 results. The nine CMIP5 models with only ARI show a drying over China and increased precipitation over India, while the models including ACI give a drying over both India and China, similar to what we find here (Figure 8h).

The clean separation into simulations with ARI-only, ACI-only and both ARI and ACI allows for an assessment of the linearity of these two processes. Looking at the regional means in Table 3, comparing the sum of ARI and ACI (see row "(ARI) + (ACI)") to the experiment including both processes ("ARI + ACI"), we find that while precipitation and downwelling shortwave radiation are close to linear, temperature is not. By closer inspection, this nonlinearity originates from the northernmost latitudes of this region, for which ARI or ACI individually

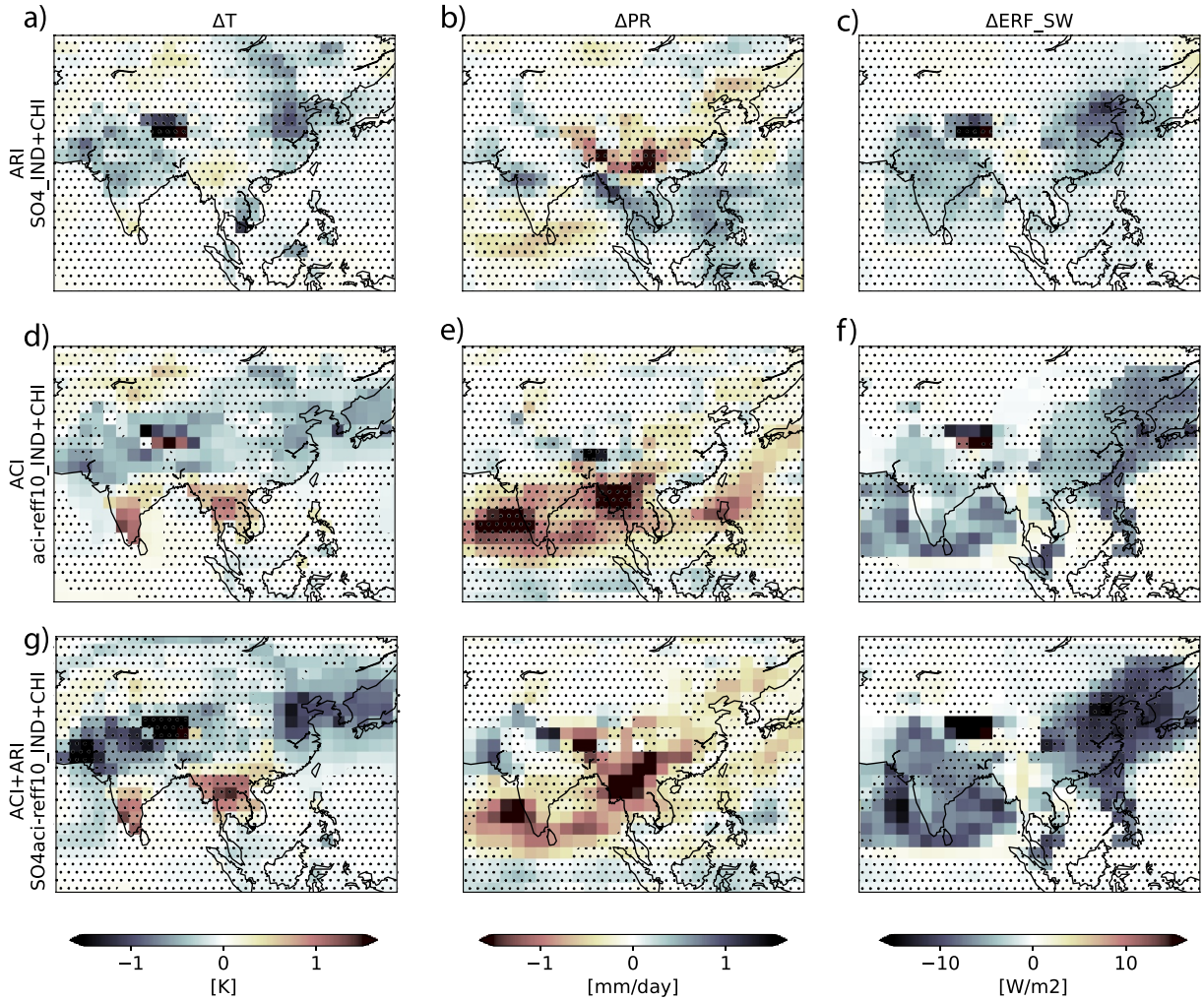

Figure 8. Summer (JJA) response to direct aerosol radiation interactions (ARI) due to Asian SO_4 (ARI, top row), as in the default setup in FORTE2, to aerosol-cloud interactions (ACI) due to Asian SO_4 (ACI, middle row) of sulfate as represented, and both the response to Asian SO_4 including both ARI and ACI (bottom row). Maps are based on years 51–200 of the simulations, and hatched regions show areas where differences from the baseline are statistically insignificant (by Student's *t*-test, *p*-value 0.05).

cause warming (Figures 8a and 8d), but which cools when both ARI and ACI operate simultaneously (Figure 8g). Remote impacts of including the ACI effect, as well as nonlinearities, can be seen in the global maps in Figure S3 in Supporting Information S1. For instance, while both the ARI and ACI effects cause a similar pattern of remote

Table 3
Regional Mean JJA Impacts of the Different Aerosol-Cloud Interactions Simulations, As Well As the Aerosol Radiation Interactions Only Simulation (Topmost Table Row)

	Experiment name	Temp. (K)	Prec. (mm/day)	Surf. SW (W/m^2)	ERF_SW (W/m^2)
ARI	$SO4_{IND+CHI}$	−0.10	0.003	−1.92	−1.61
ACI	$aci\text{-}reff10_{IND+CHI}$	−0.05	−0.30	−2.98	−2.16
(ARI) + (ACI)	$SO4aci\text{-}reff10_{IND+CHI}$ + $aci\text{-}reff10_{IND+CHI}$	−0.15	−0.303	−4.90	−3.77
ARI + ACI	$SO4aci\text{-}reff10_{IND+CHI}$	−0.35	−0.29	−4.79	−4.48
ACI_13um	$aci\text{-}reff13_{IND+CHI}$	−0.04	−0.06	−1.28	−0.87
ARI + ACI_13um	$SO4aci\text{-}reff13_{IND+CHI}$	−0.31	−0.19	−2.73	−2.95

Note. Changes are relative to the piC simulation and are averaged over the ACI region shown in Figure 1g.

warming over the eastern parts of USA and Canada, the combined impact of these effects does not include such a warming (compare lower two rows of Figure S3 in Supporting Information S1). Likely, the "double" kick to the system is strong enough to trigger a different set of circulation responses including a more unified cooling over the entire North American region.

The SyRAP-FORTE2 setup also allows for testing how important the uncertainty in ACI is for the simulated response to aerosol forcing in this region. In the present study, we have tested the sensitivity to the emulated aerosol-induced cloud radius reduction (which in the default setup is reduced from 15 to 10 μm) by performing additional experiments only reducing the droplet radius to 13 μm. Although the relative droplet radius reduction change between default ACI and sensitivity ACI experiments is only 2 μm, the radiative impacts (Surf. SW and ERF_SW in Table 3) are almost halved. Though a large difference, this is not necessarily unrealistic, as the effect on radiation tends not to scale linearly with effective cloud radius (Boers & Rotstayn, 2001). While we also find that the difference in ACI impact on precipitation between these two experiments is substantial, the temperature change is almost the same between the experiments (−0.05 K for the default ACI experiment, and −0.04 K for the sensitivity experiment). We also note that the difference in precipitation impacts from ARI + ACI in default versus sensitivity setup is much smaller than when comparing only ACI impacts. Clearly, many nonlinear processes are involved between an initial droplet change, the radiative impact and resulting changes to meteorological variables.

5.3. Regional Linearity of the Perturbations

There are many examples of idealized model simulations of regional aerosol perturbations in the literature, and some of these studies have investigated the regional linearity or additivity of the climate responses. A recent example is Herbert et al. (2022), who used the atmospheric component of FORTE2 and performed separate simulations removing BC or SO_4 from India or China. In stark contrast to our results, they find strongly nonlinear responses in the summer monsoon precipitation. H. Chen et al. (2020) also conclude, after comparing regional climate model simulations adding BC to India, China or both combined, that responses to BC are highly nonlinear. In contrast, Recchia and Lucarini (2023), also using a reduced-complexity model but using prescribed heating as a proxy for BC, find relatively linear responses in idealized experiments emulating the addition of BC aerosols over India, China, and Southeast Asia separately or at once. Westervelt et al. (2015) too, combining results from three ESMs, found that the regional responses to global perturbations to different aerosol species could be linearly superposed.

Here, we investigate the regional linearity in BC/SO_4 perturbations by comparing the added impacts of BC/SO_4 perturbations over IND and CHI to experiments where we perturb BC/SO_4 over both regions at once. Figures 9e and 9f illustrates the nonlinearity to BC perturbations in the two regions. Positive values mean that adding BC to both regions at once triggers a stronger response than the sum of responses when adding BC to the two regions individually. As indicated by the hatchings in Figures 9e and 9f, the regional BC perturbations are significantly nonlinear only in a very small region in Northern India. As can be seen by comparing the individual maps, this region is typically a transitional region between different climate responses. It is also a region of complex topography, and Herbert et al. (2022) showed that different circulation patterns interacting with the orography was a key factor for the nonlinearity of the response.

Nonlinearities in responses to SO_4 (right half of Figure 9) are slightly larger than for BC. Significant nonlinearities are, like for BC, present over parts of Northern India, but also over China around the same latitudes (Figures 9k and 9l). In particular, when SO_4 is added to both CHI and IND at once (Figure 9i) there is a small cooling over China not present in the added responses (Figure 9g). Looking back at Figure 7d we see that adding SO_4 to India alone caused a statistically significant warming over China, and this warming is associated with a region of significant anomalous descent (not shown) and reduction in mid-level clouds (Figure S4 in Supporting Information S1). To summarize, some processes are only evident when particularly SO_4 is added to a specific region, and not necessarily when adjacent regions are cooled by SO_4 simultaneously. In general, the responses to BC perturbations are broadly linear in FORTE2, while SO_4 perturbations display more nonlinearity. This means that the SyRAP-FORTE2 simulations are better suited for Green's function type studies for BC than SO_4.

As IGCM4 used by Herbert et al. (2022) is FORTE's atmospheric component, their much stronger nonlinearity is surprising. One possible cause of this disparity could be the substantially larger spatial extent of our forcing. To test this, we performed an additional version of the IND experiment where the IND region was limited to the

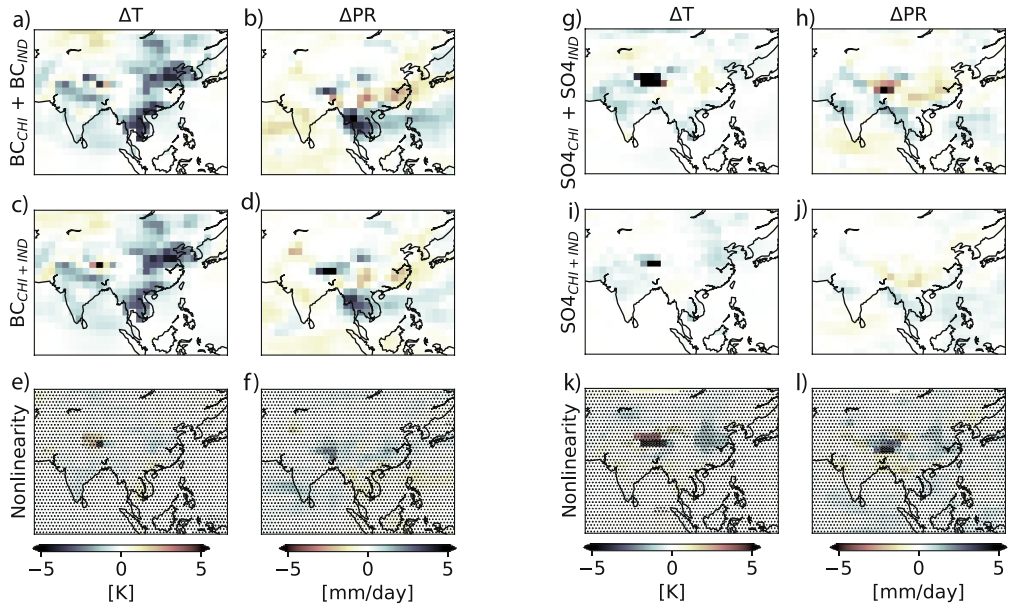

Figure 9. The linearity of mean summer (JJA) temperature and precipitation responses to black carbon and SO_4. Topmost row shows the sum of the responses from the individual regional experiments, middle row show responses from and experiment where aerosol is added to both IND and CHI at once, and bottom row shows the difference between the two above, thus quantifying the nonlinearity. Maps are based on years 51–200 of the simulations, and grid cells with statistically significant nonlinearity are indicated by absence of hatchings.

Northern parts of India only, more similar to Herbert et al. (Table 1). Compare black dashed (IND) and dotted line (NIND) in Figure 1a. However, as seen in Figure S5 in Supporting Information S1, results are no less linear with this smaller perturbation region. Instead, this discrepancy might arise from the fact that our simulations are fully coupled to an ocean model, or it may be related to the simulation design (for instance, Herbert et al. (2022) remove aerosols from a present-day climate and aerosols field, while we add aerosols to a preindustrial climate with no aerosols). Either way, the linearity allows for the utilization of these simulations in an additive manner in this case Linearity would need to be assessed for other models adopting a SyRAP approach as a degree of model dependence is also likely, since the nonlinearity is tied to the dynamical component of the response to aerosol.

5.4. Aerosol Impacts on Asian Climate for Different Climate States

In the core simulations presented in Section 3, aerosols were perturbed on top of a preindustrial climate (piC) in terms of CO_2 levels (280 ppmv). However, in both the present-day as well as the future, the climate will be in a different state, notably with higher concentrations of CO_2 and higher average temperatures. In a separate set of simulations, we have investigated how the Asian climate responds to BC and SO_4 aerosols on top of a climate that is one degree warmer (+1 K; CO_2 level at 500 ppmv) than in our core simulations. Comparing these sets of simulations allows an assessment of whether different climate responses to aerosols can be expected to emerge as climate warms.

In general, BC aerosols cause similar geographical precipitation response patterns as climate warms (compare rows in the leftmost half of Figure 10). The lowermost row indicates that adding BC to China in the different climates does not lead to significant differences in precipitation responses in any widespread subregions, while adding BC to India leads to a significantly weaker precipitation increase over Myanmar and Thailand in the warmer climate.

In both SO_4 experiments, we see stronger differences in the precipitation response between the different climates. Adding SO_4 over India causes a drying over the Himalayas and the south tip of India in the preindustrial climate but not in the warmer climate. A similar effect in the Himalayan region can be seen for SO_4 over China, but the starkest difference is found over Myanmar and Thailand. In the preindustrial climate the Indian SO_4 triggers a

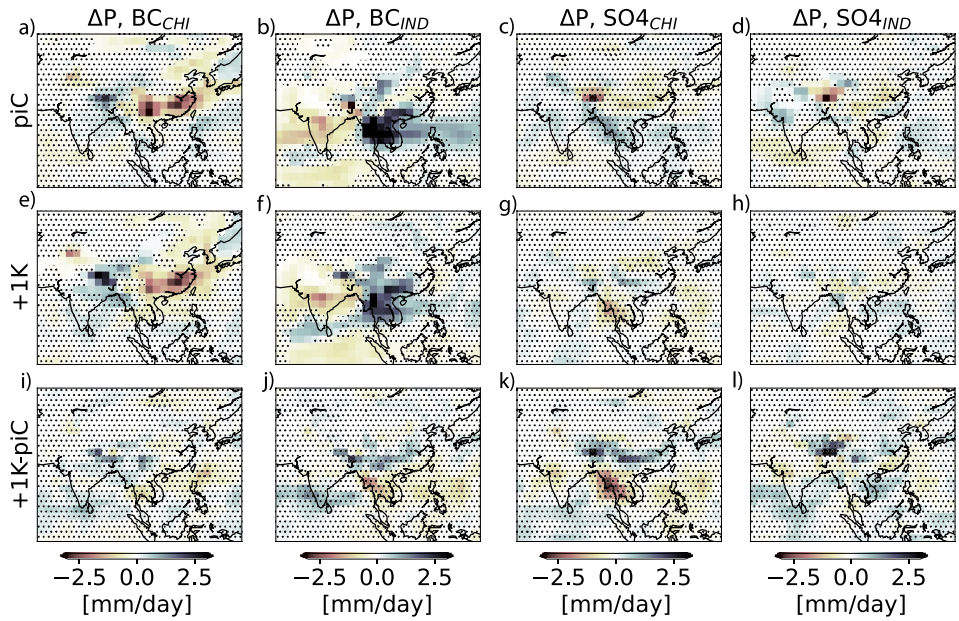

Figure 10. Mean summer (JJA) responses in precipitation in a preindustrial climate (upper row), a 1° warmer climate (middle row) and the difference between the two (bottom row). Maps are based on years 51–200 of the simulations. Note that hatching in the two first lines indicate where the aerosol response is non-significant for the given climate state, while hatching on the bottom line indicates where the difference between the aerosol responses in the two different climates are not statistically significant.

precipitation increase, while in the warmer climate the signal changes sign and becomes a drying. This sensitivity of the SO_4 response to the background climate underlines the importance of the simulation setup when studying aerosol-climate interactions, and also how inferences drawn about sensitivities to aerosol emissions in today's climate may not hold for future levels of global warming. This remains a largely unquantified source of uncertainty in future projections of aerosol emission influences.

6. Conclusions

Aerosol climate impacts can follow patterns and time evolutions that are different to those from greenhouse gas driven global surface warming, potentially enhancing climate risk when combined with regionally differing socioeconomic factors. However, our understanding of these aerosol specific patterns and processes is still limited. For instance, in Asia, a high population density in combination with high water stress makes the region vulnerable, in particular to changes in precipitation. Recognizing this vulnerability, many previous model studies have analyzed impacts of different types of aerosols from different Asian subregions, studied the role of direct versus indirect aerosol effects, or explored how specific aerosol impacts change in a changing climate.

In this work, using a reduced-complexity climate model, we address all these processes, allowing for a comparison of the relative importance of the different effects. We note that the simplified model as well as experiment design means that while most of the key processes are included here, there are certain caveats. For instance, prescribed aerosol concentrations preclude wet deposition feedbacks that could both amplify and dampen the responses in a more realistic setup. However, we also document here the inclusion of an aerosol-cloud interaction treatment in FORTE2, and its influence on the modeled responses to aerosol emissions, resolving a major known shortcoming of the model to-date. With those limitations in mind, we show how a set of systematic aerosol emission perturbations in a reduced-complexity climate model can be used to identify physical responses to regionalized aerosol emissions, with a range of physical properties, and that it is possible to combine these into a tool for building hypotheses about the joint influence of baskets of aerosol emission types.

We found that perturbations of absorbing or scattering aerosols in FORTE2 reproduce important features already shown in the literature, based on observations, and on simulations using more complex ESMs. We

find that the presence of black carbon (BC) and sulfate (SO_4) aerosols in China and India cause local reductions in surface solar radiation that trigger thermodynamic responses, leading to changes in temperature, surface fluxes and precipitation. The dynamical responses in pressure, winds, and circulation patterns contribute to changes in clouds and precipitation and have widespread impacts outside the perturbed areas. Adding BC over China causes a strong local precipitation reduction. BC over India also causes local drying but a strong increase in precipitation over Southeast Asia. Adding SO_4 over China leads to reduced precipitation locally, while SO_4 over India leads to increased precipitation in northwestern India and warming and drying over East China.

The same amount of BC or SO_4 aerosols cause weaker near-surface cooling and precipitation changes in a warmer climate. However, the geographical distribution of precipitation changes on a sub-regional scale reveal important differences. For instance, SO_4 over China causes increased precipitation over Southeast Asia in a preindustrial climate, but in a warmer climate, the precipitation impact of SO_4 on this region changes sign entirely.

The inclusion of ACI strengthens the modeled response to sulfate aerosols, by increasing the magnitude and spatial extent of their interaction with shortwave radiation. In particular, including ACI contributes to a warming as well as drying effect over Southern India and South Asia. For BC aerosols, which make a smaller contribution to the total aerosol number than SO_4 and have previously been shown to influence climate primarily through direct scattering and absorption of radiation (Bond et al., 2013), ACI is not yet implemented in FORTE2. This is a potential avenue for further development, in order fully represent the processes that link BC to local and remote climate effects, however it is expected to be of secondary importance. Adding the separate response to a given aerosol impact in the two different regions (IND and CHI) are comparable to the impact of adding aerosols to both regions at once. In other words, responses are reasonably linear, which makes the SyRAP simulations well suited as a tool for understanding joint influences of multiple aerosol-driven climate forcings. While the focus of our work has been on Asia, and the regions home to the current dominant emitters of anthropogenic aerosols, similar studies for other regions would be highly useful as a future exercise. They could also include the responses to natural aerosol sources such as dust, biomass burning and sea salt, expected to become more important as we transition into a post-fossil future with a warmer global climate.

Data Availability Statement

The present analyses is based on model simulations using the FORTE2 (version v2.0) reduced-complexity climate model. The model is freely available for download (Blaker et al., 2020). Aerosol perturbation simulations use AOD from the CAMSRA, as detailed in the Methods section. The Copernicus Atmosphere Monitoring Reanalysis (CAMSRA) was downloaded from the CAMS Atmosphere Data Store (ADS) (CAMS-EAC4, 2019, 2020; Inness et al., 2019). Figure 5 compares FORTE2 sea level pressure and winds to that from ERA5 reanalysis (Hersbach et al., 2020). All FORTE2 model results are available for download at the repository NIRD Research Data Archive (Stjern, 2024). Python code for analysis of the FORTE2 results as well as for plotting figures in the manuscript will be available for download at the same repository.

References

Allen, M. R., & Ingram, W. J. (2002). Constraints on future changes in climate and the hydrologic cycle. *Nature*, *419*(6903), 228–232. https://doi.org/10.1038/nature01092

Allen, R. J. (2000). *ENSO: Multiscale variability and global and regional impacts*. Cambridge University Press.

Allen, R. J., Turnock, S., Nabat, P., Neubauer, D., Lohmann, U., Olivié, D., et al. (2020). Climate and air quality impacts due to mitigation of non-methane near-term climate forcers. *Atmospheric Chemistry and Physics*, *20*(16), 9641–9663. https://doi.org/10.5194/acp-20-9641-2020

Allen, R. J., & Zhao, X. (2022). Anthropogenic aerosol impacts on Pacific Coast precipitation in CMIP6 models. *Environmental Research: Climate*, *1*, 015005. https://doi.org/10.1088/2752-5295/ac7d68

Blaker, A., Joshi, M., Sinha, B., Stevens, D., Smith, R., & Hirschi, J. (2020). NOC-MSM/FORTE2.0: FORTE 2.0: A fast, parallel and flexible coupled climate model (v2.0) [Dataset]. *Zenodo*. https://doi.org/10.5281/zenodo.3632569

Blaker, A. T., Joshi, M., Sinha, B., Stevens, D. P., Smith, R. S., & Hirschi, J. J. M. (2021). FORTE 2.0: A fast, parallel and flexible coupled climate model. *Geoscientific Model Development*, *14*(1), 275–293. https://doi.org/10.5194/gmd-14-275-2021

Boers, R., & Rotstayn, L. D. (2001). Possible links between cloud optical depth and effective radius in remote sensing observations. *Quarterly Journal of the Royal Meteorological Society*, *127*(577), 2367–2383. https://doi.org/10.1002/qj.49712757709

Bollasina, M. A., Ming, Y., & Ramaswamy, V. (2011). Anthropogenic aerosols and the weakening of the South Asian summer monsoon. *Science*, *334*(6055), 502–505. https://doi.org/10.1126/science.1204994

Bond, T. C., Doherty, S. J., Fahey, D. W., Forster, P. M., Berntsen, T., DeAngelo, B. J., et al. (2013). Bounding the role of black carbon in the climate system: A scientific assessment. *Journal of Geophysical Research: Atmospheres*, *118*(11), 5380–5552. https://doi.org/10.1002/jgrd.50171

CAMS-EAC4. (2019). CAMS global reanalysis (EAC4) monthly averaged fields. Retrieved from https://ads.atmosphere.copernicus.eu/cdsapp#!/dataset/cams-global-reanalysis-eac4-monthly?tab=overview

Acknowledgments

We acknowledge the Center for Advanced Study in Oslo, Norway that funded and hosted our HETCLIF centre during the academic year of 2023/24. The research presented in this paper was carried out on the high-performance computing cluster supported by the Research and Specialist Computing Support service at the University of East Anglia, UK. Data were stored and shared on project account NS9188KK on resources provided by UNINETT Sigma2—the National Infrastructure for High Performance Computing and Data Storage in Norway. All coauthors were supported by the Research Council of Norway [Grant 324182 (CA^3THY)].

CAMS-EAC4. (2020). CAMS global reanalysis (EAC4). Retrieved from https://ads.atmosphere.copernicus.eu/cdsapp#!/dataset/cams-global-reanalysis-eac4

Chen, H., Zhuang, B., Liu, J., Li, S., Wang, T., Xie, X., et al. (2020). Regional climate responses in East Asia to the black carbon aerosol direct effects from India and China in summer. *Journal of Climate*, *33*(22), 9783–9800. https://doi.org/10.1175/JCLI-D-19-0706.1

Chen, S., Chen, W., Yu, B., & Wu, R. (2023). How well can current climate models simulate the connection of the early spring Aleutian low to the following winter ENSO? *Journal of Climate*, *36*(2), 603–624. https://doi.org/10.1175/JCLI-D-22-0323.1

Chen, W., Dong, B., Wilcox, L., Luo, F., Dunstone, N., & Highwood, E. J. (2019). Attribution of recent trends in temperature extremes over China: Role of changes in anthropogenic aerosol emissions over Asia. *Journal of Climate*, *32*(21), 7539–7560. https://doi.org/10.1175/jcli-d-18-0777.1

Cook, J., & Highwood, E. J. (2004). Climate response to tropospheric absorbing aerosols in an intermediate general-circulation model. *Quarterly Journal of the Royal Meteorological Society*, *130*(596), 175–191. https://doi.org/10.1256/qj.03.64

Davey, M. K., Brookshaw, A., & Ineson, S. (2014). The probability of the impact of ENSO on precipitation and near-surface temperature. *Climate Risk Management*, *1*, 5–24. https://doi.org/10.1016/j.crm.2013.12.002

Dittus, A. J., Hawkins, E., Robson, J. I., Smith, D. M., & Wilcox, L. J. (2021). Drivers of recent North Pacific decadal variability: The role of aerosol forcing. *Earth's Future*, *9*(12), e2021EF002249. https://doi.org/10.1029/2021EF002249

Dong, B., Sutton, R. T., Highwood, E. J., & Wilcox, L. J. (2016). Preferred response of the East Asian summer monsoon to local and non-local anthropogenic sulphur dioxide emissions. *Climate Dynamics*, *46*(5–6), 1733–1751. https://doi.org/10.1007/s00382-015-2671-5

Dong, B., Wilcox, L. J., Highwood, E. J., & Sutton, R. T. (2019). Impacts of recent decadal changes in Asian aerosols on the East Asian summer monsoon: Roles of aerosol–radiation and aerosol–cloud interactions. *Climate Dynamics*, *53*(5–6), 3235–3256. https://doi.org/10.1007/s00382-019-04698-0

Fahrenbach, N. L. S., Bollasina, M. A., Samset, B. H., Cowan, T., & Ekman, A. M. L. (2024). Asian anthropogenic aerosol forcing played a key role in the multidecadal increase in Australian summer monsoon rainfall. *Journal of Climate*, *37*(3), 895–911. https://doi.org/10.1175/JCLI-D-23-0313.1

Fan, J., Rosenfeld, D., Yang, Y., Zhao, C., Leung, L. R., & Li, Z. (2015). Substantial contribution of anthropogenic air pollution to catastrophic floods in Southwest China. *Geophysical Research Letters*, *42*(14), 6066–6075. https://doi.org/10.1002/2015GL064479

Ferraro, A. J., Highwood, E. J., & Charlton-Perez, A. J. (2014). Weakened tropical circulation and reduced precipitation in response to geo-engineering. *Environmental Research Letters*, *9*(1), 014001. https://doi.org/10.1088/1748-9326/9/1/014001

Forster, P., Storelvmo, T., Armour, K., Collins, W., Dufresne, J.-L., Frame, D., et al. (2021). The Earth's energy budget, climate feedbacks, and climate sensitivity. In V. Masson-Delmotte, P. Zhai, A. Pirani, S. L. Connors, C. Péan, S. Berger, et al. (Eds.), *The Physical Science Basis. Contribution of Working Group I to the Sixth Assessment Report of the Intergovernmental Panel on Climate Change* (pp. 923–1054). Cambridge University Press.

Forster, P. M., Blackburn, M., Glover, R., & Shine, K. P. (2000). An examination of climate sensitivity for idealised climate change experiments in an intermediate general circulation model. *Climate Dynamics*, *16*(10–11), 833–849. https://doi.org/10.1007/s003820000083

Gao, J., Yang, Y., Wang, H., Wang, P., Li, B., Li, J., et al. (2023). Climate responses in China to domestic and foreign aerosol changes due to clean air actions during 2013–2019. *npj Climate and Atmospheric Science*, *6*(1), 160. https://doi.org/10.1038/s41612-023-00488-y

Gillett, N. P., Wehner, M. F., Tett, S. F. B., & Weaver, A. J. (2004). Testing the linearity of the response to combined greenhouse gas and sulfate aerosol forcing. *Geophysical Research Letters*, *31*(14), L14201. https://doi.org/10.1029/2004GL020111

Giorgi, F., & Gao, X.-J. (2018). Regional earth system modeling: Review and future directions. *Atmospheric and Oceanic Science Letters*, *11*(2), 189–197. https://doi.org/10.1080/16742834.2018.1452520

Granier, C., Bessagnet, B., Bond, T., D'Angiola, A., Denier van der Gon, H., Frost, G. J., et al. (2011). Evolution of anthropogenic and biomass burning emissions of air pollutants at global and regional scales during the 1980–2010 period. *Climatic Change*, *109*(1–2), 163–190. https://doi.org/10.1007/s10584-011-0154-1

Guo, L., Turner, A. G., & Highwood, E. J. (2015). Impacts of 20th century aerosol emissions on the South Asian monsoon in the CMIP5 models. *Atmospheric Chemistry and Physics*, *15*(11), 6367–6378. https://doi.org/10.5194/acp-15-6367-2015

Guo, Y., Dong, B., & Zhu, J. (2022). Anthropogenic impacts on changes in summer extreme precipitation over China during 1961–2014: Roles of greenhouse gases and anthropogenic aerosols. *Climate Dynamics*, *60*(9–10), 2633–2643. https://doi.org/10.1007/s00382-022-06453-4

Herbert, R., Wilcox, L. J., Joshi, M., Highwood, E., & Frame, D. (2022). Nonlinear response of Asian summer monsoon precipitation to emission reductions in South and East Asia. *Environmental Research Letters*, *17*(1), 014005. https://doi.org/10.1088/1748-9326/ac3b19

Hersbach, H., Bell, B., Berrisford, P., Hirahara, S., Horányi, A., Muñoz-Sabater, J., et al. (2020). The ERA5 global reanalysis. *Quarterly Journal of the Royal Meteorological Society*, *146*(730), 1999–2049. https://doi.org/10.1002/qj.3803

Highwood, E. J., & Stevenson, D. S. (2003). Atmospheric impact of the 1783–1784 Laki Eruption: Part II Climatic effect of sulphate aerosol. *Atmospheric Chemistry and Physics*, *3*(4), 1177–1189. https://doi.org/10.5194/acp-3-1177-2003

Holben, B. N., Eck, T. F., Slutsker, I., Tanré, D., Buis, J. P., Setzer, A., et al. (1998). AERONET—A federated instrument network and data archive for aerosol characterization. *Remote Sensing of Environment*, *66*, 1–16. https://doi.org/10.1016/S0034-4257(98)00031-5

Inness, A., Ades, M., Agustí-Panareda, A., Barré, J., Benedictow, A., Blechschmidt, A. M., et al. (2019). The CAMS reanalysis of atmospheric composition. *Atmospheric Chemistry and Physics*, *19*(6), 3515–3556. https://doi.org/10.5194/acp-19-3515-2019

Joshi, M., Stringer, M., van der Wiel, K., O'Callaghan, A., & Fueglistaler, S. (2015). IGCM4: A fast, parallel and flexible intermediate climate model. *Geoscientific Model Development*, *8*(4), 1157–1167. https://doi.org/10.5194/gmd-8-1157-2015

Kaiser, J. W., Heil, A., Andreae, M. O., Benedetti, A., Chubarova, N., Jones, L., et al. (2012). Biomass burning emissions estimated with a global fire assimilation system based on observed fire radiative power. *Biogeosciences*, *9*(1), 527–554. https://doi.org/10.5194/bg-9-527-2012

Krishnamohan, K. S., Modak, A., & Bala, G. (2021). Effects of local and remote black carbon aerosols on summer monsoon precipitation over India. *Environmental Research Communications*, *3*(8), 081003. https://doi.org/10.1088/2515-7620/ac18d1

Levy, R. C., Mattoo, S., Munchak, L. A., Remer, L. A., Sayer, A. M., Patadia, F., & Hsu, N. C. (2013). The Collection 6 MODIS aerosol products over land and ocean. *Atmospheric Measurement Techniques*, *6*(11), 2989–3034. https://doi.org/10.5194/amt-6-2989-2013

Li, B., Ding, R., Li, J., Xu, Y., & Li, J. (2018). Asymmetric response of predictability of East Asian summer monsoon to ENSO. *SOLA*, *14*(0), 52–56. https://doi.org/10.2151/sola.2018-009

Li, J., Carlson, B. E., Yung, Y. L., Lv, D., Hansen, J., Penner, J. E., et al. (2022). Scattering and absorbing aerosols in the climate system. *Nature Reviews Earth & Environment*, *3*(6), 363–379. https://doi.org/10.1038/s43017-022-00296-7

Li, X., Ting, M., Li, C., & Henderson, N. (2015). Mechanisms of Asian summer monsoon changes in response to anthropogenic forcing in CMIP5 models. *Journal of Climate*, *28*(10), 4107–4125. https://doi.org/10.1175/JCLI-D-14-00559.1

Liu, C., Yang, Y., Wang, H., Ren, L., Wei, J., Wang, P., & Liao, H. (2023). Influence of spatial dipole pattern in Asian aerosol changes on East Asian summer monsoon. *Journal of Climate*, *36*(6), 1575–1585. https://doi.org/10.1175/JCLI-D-22-0335.1

Liu, J., Rühland, K. M., Chen, J., Xu, Y., Chen, S., Chen, Q., et al. (2017). Aerosol-weakened summer monsoons decrease lake fertilization on the Chinese Loess Plateau. *Nature Climate Change*, *7*(3), 190–194. https://doi.org/10.1038/nclimate3220

Liu, Y., Cai, W., Sun, C., Song, H., Cobb, K. M., Li, J., et al. (2019). Anthropogenic aerosols cause recent pronounced weakening of Asian Summer Monsoon relative to last four centuries. *Geophysical Research Letters*, *46*(10), 5469–5479. https://doi.org/10.1029/2019GL082497

Menon, S., Hansen, J., Nazarenko, L., & Luo, Y. (2002). Climate effects of black carbon aerosols in China and India. *Science*, *297*(5590), 2250–2253. https://doi.org/10.1126/science.1075159

Monerie, P.-A., Wilcox, L. J., & Turner, A. G. (2022). Effects of anthropogenic aerosol and greenhouse gas emissions on Northern Hemisphere monsoon precipitation: Mechanisms and uncertainty. *Journal of Climate*, *35*(8), 2305–2326. https://doi.org/10.1175/JCLI-D-21-0412.1

Morcrette, J.-J., Boucher, O., Jones, L., Salmond, D., Bechtold, P., Beljaars, A., et al. (2009). Aerosol analysis and forecast in the European Centre for Medium-Range Weather Forecasts Integrated Forecast System: Forward modeling. *Journal of Geophysical Research*, *114*(D6), D06206. https://doi.org/10.1029/2008JD011235

Myhre, G., Forster, P. M., Samset, B. H., Hodnebrog, Ø., Sillmann, J., Aalbergsjø, S. G., et al. (2017). PDRMIP: A precipitation driver and response model intercomparison project, protocol and preliminary results. *Bulletin of the American Meteorological Society*, *98*(6), 1185–1198. https://doi.org/10.1175/BAMS-D-16-0019.1

Myhre, G., Kramer, R. J., Smith, C. J., Hodnebrog, Ø., Forster, P., Soden, B. J., et al. (2018). Quantifying the importance of rapid adjustments for global precipitation changes. *Geophysical Research Letters*, *45*(20), 11399–11405. https://doi.org/10.1029/2018GL079474

Nicholls, Z., Meinshausen, M., Lewis, J., Corradi, M. R., Dorheim, K., Gasser, T., et al. (2021). Reduced complexity model intercomparison project phase 2: Synthesizing Earth system knowledge for probabilistic climate projections. *Earth's Future*, *9*(6), e2020EF001900. https://doi.org/10.1029/2020EF001900

Nicholls, Z. R. J., Meinshausen, M., Lewis, J., Gieseke, R., Dommenget, D., Dorheim, K., et al. (2020). Reduced Complexity Model Intercomparison Project Phase 1: Introduction and evaluation of global-mean temperature response. *Geoscientific Model Development*, *13*(11), 5175–5190. https://doi.org/10.5194/gmd-13-5175-2020

Norris, J., Hall, A., Thackeray, C. W., Chen, D., & Madakumbura, G. D. (2022). Evaluating hydrologic sensitivity in CMIP6 models: Anthropogenic forcing versus ENSO. *Journal of Climate*, *35*(21), 6955–6968. https://doi.org/10.1175/JCLI-D-21-0842.1

Persad, G., Samset, B. H., Wilcox, L. J., Allen, R. J., Bollasina, M. A., Booth, B. B. B., et al. (2023). Rapidly evolving aerosol emissions are a dangerous omission from near-term climate risk assessments. *Environmental Research: Climate*, *2*(3), 032001. https://doi.org/10.1088/2752-5295/acd6af

Persad, G. G., & Caldeira, K. (2018). Divergent global-scale temperature effects from identical aerosols emitted in different regions. *Nature Communications*, *9*(1), 3289. https://doi.org/10.1038/s41467-018-05838-6

Platnick, S., & Twomey, S. (1994). Remote sensing the susceptibility of cloud albedo to changes in drop concentration. *Atmospheric Research*, *34*(1–4), 85–98. https://doi.org/10.1016/0169-8095(94)90082-5

Popp, T., De Leeuw, G., Bingen, C., Brühl, C., Capelle, V., Chedin, A., et al. (2016). Development, production and evaluation of aerosol climate data records from European satellite observations (Aerosol_cci). *Remote Sensing*, *8*(5), 421. https://doi.org/10.3390/rs8050421

Recchia, L. G., & Lucarini, V. (2023). Modelling the effect of aerosol and greenhouse gas forcing on the South Asian and East Asian monsoons with an intermediate-complexity climate model. *Earth System Dynamics*, *14*(3), 697–722. https://doi.org/10.5194/esd-14-697-2023

Riahi, K., Rao, S., Krey, V., Cho, C., Chirkov, V., Fischer, G., et al. (2011). Rcp 8.5—A scenario of comparatively high greenhouse gas emissions. *Climatic Change*, *109*(1–2), 33–57. https://doi.org/10.1007/s10584-011-0149-y

Risser, M. D., Collins, W. D., Wehner, M. F., O'Brien, T. A., Huang, H., & Ullrich, P. A. (2024). Anthropogenic aerosols mask increases in US rainfall by greenhouse gases. *Nature Communications*, *15*(1), 1318. https://doi.org/10.1038/s41467-024-45504-8

Salzmann, M., Weser, H., & Cherian, R. (2014). Robust response of Asian summer monsoon to anthropogenic aerosols in CMIP5 models. *Journal of Geophysical Research: Atmospheres*, *119*(19), 11321–11337. https://doi.org/10.1002/2014JD021783

Samset, B. H., Lund, M. T., Bollasina, M., Myhre, G., & Wilcox, L. (2019). Emerging Asian aerosol patterns. *Nature Geoscience*, *12*(8), 582–584. https://doi.org/10.1038/s41561-019-0424-5

Samset, B. H., Myhre, G., Forster, P. M., Hodnebrog, Ø., Andrews, T., Boucher, O., et al. (2018). Weak hydrological sensitivity to temperature change over land, independent of climate forcing. *npj Climate and Atmospheric Science*, *1*, 20173. https://doi.org/10.1038/s41612-017-0005-5

Samset, B. H., Myhre, G., Forster, P. M., Hodnebrog, Ø., Andrews, T., Faluvegi, G., et al. (2016). Fast and slow precipitation responses to individual climate forcers: A PDRMIP multimodel study. *Geophysical Research Letters*, *43*(6), 2782–2791. https://doi.org/10.1002/2016GL068064

Samset, B. H., Sand, M., Smith, C. J., Bauer, S. E., Forster, P. M., Fuglestvedt, J. S., et al. (2018). Climate impacts from a removal of anthropogenic aerosol emissions. *Geophysical Research Letters*, *45*(2), 1020–1029. https://doi.org/10.1002/2017GL076079

Song, F., Zhou, T., & Qian, Y. (2014). Responses of East Asian summer monsoon to natural and anthropogenic forcings in the 17 latest CMIP5 models. *Geophysical Research Letters*, *41*(2), 596–603. https://doi.org/10.1002/2013GL058705

Sperber, K. R., Annamalai, H., Kang, I. S., Kitoh, A., Moise, A., Turner, A., et al. (2013). The Asian summer monsoon: An intercomparison of CMIP5 vs. CMIP3 simulations of the late 20th century. *Climate Dynamics*, *41*(9–10), 2711–2744. https://doi.org/10.1007/s00382-012-1607-6

Stjern, C. W. (2024). Systematic Regional Aerosol Perturbations (SyRAP) in Asia using the intermediate-resolution global climate model FORTE2 [Dataset]. In M. Joshi (Ed.), *NIRD Research Data Archive*. https://doi.org/10.11582/2024.00103

Tebaldi, C., Debeire, K., Eyring, V., Fischer, E., Fyfe, J., Friedlingstein, P., et al. (2021). Climate model projections from the Scenario Model Intercomparison Project (ScenarioMIP) of CMIP6. *Earth System Dynamics*, *12*(1), 253–293. https://doi.org/10.5194/esd-12-253-2021

Tian, F., Dong, B., Robson, J., & Sutton, R. (2018). Forced decadal changes in the East Asian summer monsoon: The roles of greenhouse gases and anthropogenic aerosols. *Climate Dynamics*, *51*(9–10), 3699–3715. https://doi.org/10.1007/s00382-018-4105-7

Wang, Z., Lin, L., Xu, Y., Che, H., Zhang, X., Zhang, H., et al. (2021). Incorrect Asian aerosols affecting the attribution and projection of regional climate change in CMIP6 models. *npj Climate and Atmospheric Science*, *4*(1), 2. https://doi.org/10.1038/s41612-020-00159-2

Webb, D. J. (1996). An ocean model code for array processor computers. *Computers & Geosciences*, *22*(5), 569–578. https://doi.org/10.1016/0098-3004(95)00133-6

Westervelt, D. M., Conley, A. J., Fiore, A. M., Lamarque, J. F., Shindell, D. T., Previdi, M., et al. (2018). Connecting regional aerosol emissions reductions to local and remote precipitation responses. *Atmospheric Chemistry and Physics*, *18*(16), 12461–12475. https://doi.org/10.5194/acp-18-12461-2018

Westervelt, D. M., Horowitz, L. W., Naik, V., Golaz, J. C., & Mauzerall, D. L. (2015). Radiative forcing and climate response to projected 21st century aerosol decreases. *Atmospheric Chemistry and Physics*, *15*(22), 12681–12703. https://doi.org/10.5194/acp-15-12681-2015

Westervelt, D. M., Mascioli, N. R., Fiore, A. M., Conley, A. J., Lamarque, J. F., Shindell, D. T., et al. (2020). Local and remote mean and extreme temperature response to regional aerosol emissions reductions. *Atmospheric Chemistry and Physics*, *20*(5), 3009–3027. https://doi.org/10.5194/acp-20-3009-2020

Wilcox, L. J., Dunstone, N., Lewinschal, A., Bollasina, M., Ekman, A. M. L., & Highwood, E. J. (2019). Mechanisms for a remote response to Asian anthropogenic aerosol in boreal winter. *Atmospheric Chemistry and Physics*, *19*(14), 9081–9095. https://doi.org/10.5194/acp-19-9081-2019

Wilcox, L. J., Highwood, E. J., Booth, B. B. B., & Carslaw, K. S. (2015). Quantifying sources of inter-model diversity in the cloud albedo effect. *Geophysical Research Letters*, *42*(5), 1568–1575. https://doi.org/10.1002/2015GL063301

Wilcox, L. J., Liu, Z., Samset, B. H., Hawkins, E., Lund, M. T., Nordling, K., et al. (2020). Accelerated increases in global and Asian summer monsoon precipitation from future aerosol reductions. *Atmospheric Chemistry and Physics Discussions*, *2020*, 1–30. https://doi.org/10.5194/acp-2019-1188

Williams, A. I. L., Stier, P., Dagan, G., & Watson-Parris, D. (2022). Strong control of effective radiative forcing by the spatial pattern of absorbing aerosol. *Nature Climate Change*, *12*(8), 735–742. https://doi.org/10.1038/s41558-022-01415-4

Xian, P., Reid, J. S., Ades, M., Benedettie, A., Colarco, P. R., da Silva, A., et al. (2023). Intercomparison of aerosol optical depths from four reanalyses and their multi-reanalysis-consensus. *EGUsphere*, *2023*, 1–35. https://doi.org/10.5194/egusphere-2023-2354

Xie, X., Myhre, G., Liu, X., Li, X., Shi, Z., Wang, H., et al. (2020). Distinct responses of Asian summer monsoon to black carbon aerosols and greenhouse gases. *Atmospheric Chemistry and Physics*, *20*, 11823–11839. https://doi.org/10.5194/acp-20-11823-2020

Xie, X., Myhre, G., Shindell, D., Faluvegi, G., Takemura, T., Voulgarakis, A., et al. (2022). Anthropogenic sulfate aerosol pollution in South and East Asia induces increased summer precipitation over arid Central Asia. *Communications Earth & Environment*, *3*(1), 328. https://doi.org/10.1038/s43247-022-00660-x

Yang, Y., Ren, L., Wu, M., Wang, H., Song, F., Leung, L. R., et al. (2022). Abrupt emissions reductions during COVID-19 contributed to record summer rainfall in China. *Nature Communications*, *13*(1), 959. https://doi.org/10.1038/s41467-022-28537-9

Zelinka, M. D., Andrews, T., Forster, P. M., & Taylor, K. E. (2014). Quantifying components of aerosol-cloud-radiation interactions in climate models. *Journal of Geophysical Research: Atmospheres*, *119*(12), 7599–7615. https://doi.org/10.1002/2014JD021710

Zelinka, M. D., Smith, C. J., Qin, Y., & Taylor, K. E. (2023). Comparison of methods to estimate aerosol effective radiative forcings in climate models. *Atmospheric Chemistry and Physics*, *23*(15), 8879–8898. https://doi.org/10.5194/acp-23-8879-2023

Zhang, X. Y., Wang, Y. Q., Niu, T., Zhang, X. C., Gong, S. L., Zhang, Y. M., & Sun, J. Y. (2012). Atmospheric aerosol compositions in China: Spatial/temporal variability, chemical signature, regional haze distribution and comparisons with global aerosols. *Atmospheric Chemistry and Physics*, *12*(2), 779–799. https://doi.org/10.5194/acp-12-779-2012